



Published in final edited form as:

*Nat Neurosci.* 2017 December ; 20(12): 1734–1743. doi:10.1038/s41593-017-0012-1.

## A craniofacial-specific monosynaptic circuit enables heightened affective pain

Erica Rodriguez<sup>1</sup>, Katsuyasu Sakurai<sup>1</sup>, Jennie Xu<sup>1</sup>, Yong Chen<sup>2</sup>, Koji Toda<sup>3</sup>, Shengli Zhao<sup>1</sup>, Bao-Xia Han<sup>1</sup>, David Ryu<sup>1</sup>, Henry Yin<sup>3</sup>, Wolfgang Liedtke<sup>2</sup>, and Fan Wang<sup>1,\*</sup>

<sup>1</sup>Department of Neurobiology, Duke University Medical Center, Durham, North Carolina, USA

<sup>2</sup>Department of Neurology, Duke University Medical Center, Durham, North Carolina, USA

<sup>3</sup>Department of Psychology and Neuroscience, Duke University, Durham, North Carolina, USA

### Abstract

Humans often rank craniofacial pain as more severe than body pain. Evidence suggests that a stimulus of the same intensity induces stronger pain in the face than the body. However, the underlying neural circuitry for the differential processing of facial versus bodily pain remains unknown. Interestingly, the lateral parabrachial nucleus (PB<sub>L</sub>), a critical node in the affective pain circuit, is activated more strongly by noxious stimulation of the face than the hindpaw. Using a novel activity-dependent technology called CANE developed in our lab, we identified and selectively labeled noxious stimuli-activated PB<sub>L</sub> neurons, and performed comprehensive anatomical input-output mapping. Surprisingly, a hitherto uncharacterized monosynaptic connection between cranial sensory neurons and the PB<sub>L</sub>-nociceptive neurons was uncovered. Optogenetic activation of this monosynaptic craniofacial-to-PB<sub>L</sub> projection induced robust escape/avoidance behaviors and stress calls, whereas optogenetic silencing specifically reduced facial nociception. The monosynaptic circuit revealed here provides a neural substrate for heightened craniofacial affective pain.

### Introduction

Noxious stimuli experienced by the head and facial region are detected and conveyed to the central nervous system (CNS) by sensory neurons located in the trigeminal (TG) ganglia, whereas noxious stimuli affecting extracranial regions are sensed and relayed to the CNS via

Users may view, print, copy, and download text and data-mine the content in such documents, for the purposes of academic research, subject always to the full Conditions of use: [http://www.nature.com/authors/editorial\\_policies/license.html#terms](http://www.nature.com/authors/editorial_policies/license.html#terms)

Correspondence should be addressed to F.W. ([fan.wang@duke.edu](mailto:fan.wang@duke.edu)).

#### Author Contributions

F.W. and E.R. conceived the idea and designed the experiments. E.R. performed majority of the experiments and data analysis. K.S. performed some independent CANE capture experiments, bilateral fiber implantations and the place escape/avoidance (PEA) behavioral experiments. K.T. analyzed PEA results (blind to genotype). J.X. performed immunohistochemistry, quantified axon projections, and quantified cells in Fos and transsynaptic experiments (blind to experimental conditions). Y.C. performed all the face and hindpaw von Frey assays (blind to genotypes). D.R. quantified cells in a subset of colocalization experiments. S.Z. produced all the CANE-LV and CANE-RV viruses. B.-X.H. took care of mouse husbandry and genotyping. H.Y. and W.L. provided critical equipment and reagents. F.W. and E.R. wrote the manuscript with the help from W.L.

#### Competing Financial Interests

The authors declare no competing financial interests.

primary sensory neurons residing in the dorsal root ganglia (DRG). Humans generally rank head and facial pain as much more severe and emotionally draining than body pain. For example, two of the arguably most severe chronic pain conditions are trigeminal neuralgia and cluster headaches<sup>1-3</sup>. Craniofacial pain sensation is qualitatively different from bodily nociception as shown in human experiments, where repeated application of noxious heat to the face induces sensitization, yet similar stimulation applied to the hand induced habituation<sup>4</sup>. Fear induced by pain in human subjects was rated higher for face than for extremities, despite comparable ratings of the pain intensity<sup>5</sup>. fMRI studies further revealed that face pain resulted in higher levels of amygdala activation compared to the same intensity stimulation applied to the hand<sup>6</sup>. Despite these studies, the neuro-biological underpinning for heightened craniofacial pain remained enigmatic.

“Suffering” and “fear of pain” are emotional aspects of pain that are *not* processed by the canonical discriminative pathway via the spino-thalamic-cortical somatosensory circuits. Instead, these feelings are relayed by the less-studied affective pain pathway, where nociceptive afferent information is routed from second-order neurons to the lateral parabrachial nucleus (PB<sub>L</sub>) onto various limbic regions, such as the central amygdala (CeA), the bed nucleus stria terminalis (BNST), the lateral hypothalamus (LHA), the anterior cingulate and the insular cortices (aka the spino-parabrachial circuit)<sup>7-9</sup>. Interestingly, it was suggested that subregions of the PB<sub>L</sub>, a critical relay node in the affective pain circuit, might be differentially activated by noxious stimuli applied to the face versus the extremities in rats<sup>10,11</sup>.

In this study, we show that painful stimuli applied to the face activate more PB<sub>L</sub> neurons and do so more bilaterally compared to those applied to paw. We utilize our novel activity-dependent technology called CANE<sup>12</sup> to identify PB<sub>L</sub>-nociceptive neurons and their connections with the affective pain system. We further discover the circuit mechanism underlying the more robust activation of PB<sub>L</sub> by noxious facial stimuli and show that activation of this circuit drives strong aversive behaviors, whereas inhibition specifically reduces craniofacial nociception.

## Results

### Noxious facial stimuli activate the lateral parabrachial nucleus more robustly and bilaterally compared to noxious bodily stimuli

We injected 4% formalin (a noxious chemical) either unilaterally into the whisker pad, or unilaterally into one hindpaw, and immunostained for the immediate early gene Fos as a marker for activated neurons in the PB<sub>L</sub> (Fig. 1a). Whisker pad formalin injection activated the PB<sub>L</sub> with significantly more Fos<sup>+</sup> neurons than paw injection of an equivalent amount of formalin (Fig. 1c; Whisker:  $952 \pm 100.7$ ; Paw:  $616 \pm 75.1$  total Fos<sup>+</sup> neurons;  $P = 0.04$ ;  $n = 7$ ), especially in the external lateral sub-nucleus of the PB<sub>L</sub> (PB-el) (Fig. 1b). Furthermore, unilateral formalin whisker pad injection induced Fos<sup>+</sup> neurons in PB-el *bilaterally* with a trend of more Fos<sup>+</sup> cell on the ipsilateral side (Fig. 1b, d; Contra:  $213.8 \pm 32.8$ ; Ipsi:  $281.5 \pm 22.3$  Fos<sup>+</sup> neurons;  $P = 0.053$ ;  $n = 4$ ). By contrast, unilateral paw formalin injection preferentially activated the *contralateral* PB-el with significantly more Fos<sup>+</sup> neurons on the contralateral than on the ipsilateral side (Fig. 1b, d; Contra:  $253.3 \pm 24.1$ ; Ipsi:  $129.7 \pm 14.3$

Fos<sup>+</sup> neurons;  $P < 0.01$ ;  $n = 3$ ), which is consistent with the fact that spino-parabrachial projection neurons in dorsal spinal cord are known to predominantly send axons to the contralateral side<sup>9,10</sup>. Additionally, consistent with the fact that the affective pain circuit does not discriminate the types of pain<sup>7</sup>, we found that capsaicin, formalin, and even the minor pain associated with control injection of saline unilaterally into the whisker pad all activated the PB<sub>L</sub> neurons (including neurons in PB-el) compared to no-injection controls, with formalin the most potent stimulus to evoke Fos<sup>+</sup> neurons (Supplementary Fig. 1a, b; Home Cage:  $73 \pm 26$ ; Saline:  $421 \pm 94$ ; Capsaicin:  $673 \pm 72$ ; Formalin:  $952 \pm 101$  Fos<sup>+</sup> neurons,  $n = 3,3,3,4$ ). In the same animals, we also observed Fos<sup>+</sup> neurons in spinal trigeminal nucleus caudalis (Sp5C), which was expected since Sp5C is a main relay in the trigeminal-thalamic-cortical pain pathway (Supplementary Fig. 1c,  $n = 3$ )<sup>11,13,14</sup>.

### PB<sub>L</sub> neurons activated by noxious facial stimuli are molecularly heterogeneous

Two-color fluorescence in situ hybridization further showed that most Fos<sup>+</sup> PB<sub>L</sub>-nociceptive neurons were *slc17a6+* (i.e. *vGlut2*<sup>+</sup>) (Supplementary Fig. 2a, b; glutamatergic;  $80 \pm 1\%$ ,  $n = 3$ ), while only a minority of Fos<sup>+</sup> cells were *gad1/2*<sup>+</sup> (Supplementary Fig. 2a, b; GABAergic;  $7 \pm 2\%$ ,  $n = 3$ ). A recent study showed that the gene *calca* encoding calcitonin gene-related peptide (CGRP) is expressed in PB-el<sup>15</sup>. These CGRP<sup>+</sup> PB-el neurons were activated by intense foot shock, and transmitted affective pain signals to the CeA<sup>14</sup>. We therefore decided to focus on CGRP expression and found a subset of Fos<sup>+</sup> PB<sub>L</sub>-nociceptive neurons in the ventral region indeed expressed CGRP (Supplementary Fig. 2c-d;  $56 \pm 5\%$  of ventral;  $2 \pm 1\%$  of dorsal;  $34 \pm 3\%$  of total Fos<sup>+</sup> PB<sub>L</sub>-nociceptive pain neurons were CGRP<sup>+</sup>;  $n = 3$ ). Another marker, the Forkhead box protein P2 (FoxP2), implicated in circuits related to vocal communication and sodium intake, has also been found to be expressed in the PB<sub>L</sub><sup>16,17</sup>. We found that again only a subset of Fos<sup>+</sup> PB<sub>L</sub> neurons in the dorsal region expressed FoxP2 (Supplementary Fig. 2c-d;  $9 \pm 4\%$  of ventral;  $46 \pm 10\%$  of dorsal;  $21 \pm 5\%$  of total Fos<sup>+</sup> PB<sub>L</sub>-nociceptive neurons were FoxP2<sup>+</sup>;  $n = 3$ ).

### CANE is efficient and selective in activity-dependent capturing of facial nociceptive relay PB<sub>L</sub> neurons

How might noxious facial stimuli activate more neurons in the PB<sub>L</sub>, particularly in the PB-el, compared to noxious bodily stimuli, especially on the *ipsilateral* side? To answer this question, we needed to identify neurons that provide presynaptic inputs to face-nociception-activated PB<sub>L</sub> neurons. Previous studies using anterograde and retrograde tracer dyes labeled the general afferents to the entire PB<sub>L</sub> region<sup>9,13,14,18,19</sup>. However, the PB<sub>L</sub> contains diverse populations of neurons in addition to neurons responsive to noxious stimuli, such as cells activated by innocuous warm and cool temperatures, as well as cells responsive to various taste stimuli<sup>20,21</sup>. The PB<sub>L</sub> is also known for its significant role in regulating instinctive behavior, namely thirst for water, sodium appetite and hunger for food<sup>22-24</sup>. Thus, tracer based studies lack the resolution to identify specific inputs to the PB<sub>L</sub>-nociceptive neurons. Since CGRP and FoxP2 only label subsets of PB<sub>L</sub>-nociceptive neurons (Supplementary Fig. 2c-d), we reasoned that transsynaptic tracing of inputs to either CGRP<sup>+</sup> or FoxP2<sup>+</sup> neurons may miss certain types of inputs that innervate the non-CGRP<sup>+</sup>, or non-FoxP2<sup>+</sup> PB<sub>L</sub>-nociceptive neurons. We therefore turned to our newly developed technology called CANE for viral-genetic tagging of transiently-activated neurons to capture noxious stimuli-activated

PB<sub>L</sub> neurons. CANE uses a pseudotyped lentivirus or rabies virus to selectively infect Fos<sup>+</sup> neurons genetically engineered to transiently express the receptor for the pseudotyped viruses (Fos<sup>TV</sup>A mice), and consequently, the viruses mediate expression of desired transgenes in activated cells<sup>12</sup>.

We first validated that CANE could indeed selectively label PB<sub>L</sub>-nociceptive neurons. In a two-bout experimental paradigm, CANE was used to capture PB<sub>L</sub> neurons activated by a noxious stimulus (capsaicin or formalin injection) by co-injecting CANE-LV-Cre and AAV-flex-GFP into the PB<sub>L</sub>. Three weeks later, the same animal was given a second painful stimulus to induce Fos expression and sacrificed for immunostaining (Fig. 2a). In both capsaicin-capsaicin, and formalin-formalin paradigms, 55 ± 3% (n=9) and 55 ± 2% (n=9) of CANE-captured PB<sub>L</sub> neurons were Fos<sup>+</sup>, respectively (Fig. 2 d, f, h, i). This indicated that the second noxious injection reactivated many (~55%) of the same cells excited by the first stimulus. By contrast, without noxious stimulation, there was only a small number of background captured neurons (due to Fos-expression in PB<sub>L</sub> induced by handling/restraining the animals but without application of noxious stimuli), which had significantly less overlap with Fos<sup>+</sup> neurons induced by noxious stimuli (Fig. 2b, e, h, i; 27 ± 3% CANE<sup>+</sup> cells were Fos<sup>+</sup> in no stimulus-formalin paradigm (n=5; P < 0.0001); 31 ± 5% CANE<sup>+</sup> cells were Fos<sup>+</sup> in the no stimulus-capsaicin paradigm (n=4; P < 0.0001)). In the capsaicin-saline paradigm, 36 ± 3% CANE-captured cells were Fos<sup>+</sup> activated by saline injection (Fig. 2e, h, n=4; P = 0.0005), consistent with the fact that saline injection only caused moderate PB<sub>L</sub> activation. Previous electrophysiological studies reveal that the same PB<sub>L</sub> neurons could be activated by different noxious modalities<sup>25</sup>, prompting us to ask whether CANE-captured capsaicin-activated PB<sub>L</sub> neurons overlapped with formalin-activated neurons and vice versa. Indeed, we observed a similar percentage of CANE<sup>+</sup> neurons that were Fos<sup>+</sup> regardless of whether the capsaicin-formalin paradigm was used (51 ± 2%; n = 7) or vice-versa (55 ± 2%; n = 6) (Fig. 2c, h, i). We also examined the overlap between CANE-captured face-activated PB<sub>L</sub>-nociceptive neurons and Fos<sup>+</sup> cells induced by contralateral hindpaw nociception and vice versa. About 30% of CANE<sup>+</sup> neurons were Fos<sup>+</sup> in both whisker-hindpaw and hindpaw-whisker nociception paradigms (Fig. 2g, j; W:H, 26 ± 3%; H:W, 33 ± 4%, n = 6). Our observations are consistent with the current concept that the PB<sub>L</sub> mediated affective pain circuit plays a limited role in discriminating the types and locations of injury<sup>25,26</sup>. As an additional control for the specificity of CANE, we co-injected CANE-LV-Cre, AAV-flex-GFP (CANE::GFP), and AAV-tdTomato into the PB<sub>L</sub> after formalin injection into the whisker pad, and compared the labeling resulted from the two viral methods. CANE::GFP labeled a specific subset of PB<sub>L</sub> neurons, whereas AAV-tdTomato labeled a majority of neurons at the injection site (Supplementary Fig. 3, n = 4), thus further confirming the specificity of our method.

### **PB<sub>L</sub>-nociceptive neurons project axons to multiple emotion- and instinct-related centers in the brain**

We next traced the axonal projections of CANE::GFP-captured PB<sub>L</sub>-nociceptive neurons. The targets of PB<sub>L</sub>-nociceptive neurons include: the bed nucleus of the stria terminalis (BNST, where PB<sub>L</sub> axons form large axonal boutons surrounding BNST neuron cell bodies), the paraventricular thalamic nucleus (PVT), the paraventricular nucleus of the hypothalamus

(PVH), CeAc (the capsular division), the ventral tegmental area (VTA), the ventrolateral periaqueductal grey (PAG<sub>vl</sub>), the nucleus of the solitary tract (NST) and the intermediate reticular nucleus in the hindbrain (IRt) (Fig. 2k-r). Quantitative measurements of the densities of innervation (n = 3) using a previously described method<sup>12,27</sup> showed that the majority of projections were ipsilateral with small numbers of axons innervating the contralateral side (Fig. 2q). A schematic summary of the projections is shown (Fig. 2r). Notably, all the targets of PB<sub>L</sub>-nociceptive neurons contained Fos<sup>+</sup> neurons induced by noxious facial stimulation (Fig. 2k-p, green signals).

### **PB<sub>L</sub>-nociceptive neurons receive reciprocal inputs from emotion-related limbic regions and bilateral inputs from various reticular brainstem regions**

Having validated that CANE selectively captured PB<sub>L</sub>-nociceptive neurons that relay signal to emotion- and instinct-related centers, we mapped the presynaptic inputs to these neurons using a CANE-based transsynaptic tracing method<sup>12</sup>. Briefly, CANE-LV-Cre and the helper virus AAV-SynP-DIO-TVA-EGFP-RG<sup>28</sup> were co-injected into the ipsilateral PB<sub>L</sub> to express the TVA receptor, rabies glycoprotein G, and GFP selectively in the PB<sub>L</sub> neurons which were activated by formalin injection into the whisker pad. Two weeks later, CANE-RV-mCherry was injected into the same location in PB<sub>L</sub>. The GFP/mCherry double-positive neurons are the starter PB<sub>L</sub>-nociceptive neurons, while mCherry<sup>+</sup> neurons outside of the PB<sub>L</sub> are presynaptic neurons (Fig. 3a, b). We observed mCherry<sup>+</sup> neurons in BNST, CeAm (medial division), and several hypothalamic nuclei including the PVH, substantia nigra pars compacta (SNpc), PAG<sub>vl</sub>, brainstem reticular regions, NST, spinal trigeminal nucleus caudalis (Sp5C), and the dorsal horn of the spinal cord (Fig. 3c-j, m; quantification represents numbers of labeled presynaptic neurons/number of starter neurons; n = 6). Note that the labeled neurons in the reticular regions, NST, and Sp5C neurons were distributed bilaterally with an ipsilateral dominance (Fig. 3m; number of transsynaptically labeled cells/number of starter cell: Ipsi. [IRt: 6.3 ± 1.3; PCRt: 6.4 ± 1.4; MRn: 1.3 ± 0.4; GRn: 3.1 ± 0.7; NST: 1.9 ± 0.7; Sp5C: 5.3 ± 1.6]; Contra. [IRt: 0.9 ± 0.2; PCRt: 1.4 ± 0.5; MRn: 3.8 ± 0.8; GRn: 2.1 ± 0.5; NST: 0.8 ± 0.2; Sp5C: 0.5 ± 0.2]), consistent with previous dye tracing studies<sup>9,13,14,18,19</sup>. Additionally, there were a few labeled cells in the contralateral PB<sub>L</sub> (Fig. 3m; 0.7 ± 0.2). A schematic summary of the projections is shown (Fig. 3o).

### **CANE-captured PB<sub>L</sub>-nociceptive neurons receive direct input from primary sensory neurons in the ipsilateral trigeminal ganglion**

Interestingly, transsynaptically labeled mCherry<sup>+</sup> neurons were also observed in the *ipsilateral* TG, but not in any of the DRG on either side (n = 6, Fig. 3k, l), suggesting that TG sensory neurons innervating head and face provide direct monosynaptic inputs to *ipsilateral* PB<sub>L</sub>-nociceptive neurons. A few previous anatomical studies hinted at the possibility of a direct TG-PB connection<sup>29–32</sup>. Interestingly, transsynaptic tracing of inputs to hindpaw formalin-activated PB<sub>L</sub>-nociceptive neurons also revealed labeled neurons in TG but not in any DRG (n = 4, Fig. 3n), suggesting craniofacial but not body primary sensory neurons provide direct, monosynaptic inputs onto PB<sub>L</sub>-nociceptive neurons. The result is also consistent with the idea that some PB<sub>L</sub>-nociceptive neurons receive convergent inputs from both face and body. We examined the expression of IB4 (a marker for non-peptidergic c fibers), CGRP, TrpV1 (the receptor for capsaicin and a marker for a subset of c fibers and a

small subset of A $\delta$  fibers), and NF200 (a marker for both A $\delta$  and A $\beta$  fibers) among the transsynaptically labeled TG neurons. The TG neurons directly presynaptic to the PB<sub>L</sub> included NF200<sup>+</sup> (45  $\pm$  4%), TrpV1<sup>+</sup> (38.5  $\pm$  4%), CGRP<sup>+</sup> (26.2  $\pm$  7%), and IB4<sup>+</sup> cells (12  $\pm$  4%; n = 8; Fig. 3p, q). Taken together, the transsynaptic tracing studies suggest that there are two separate pathways transmitting craniofacial nociception from TG to the PB<sub>L</sub>: (1) the previously known indirect TG  $\rightarrow$  Sp5C  $\rightarrow$  PB<sub>L</sub> and (2) the newly revealed direct TG  $\rightarrow$  PB<sub>L</sub> projection. By contrast, there is only one indirect pathway transmitting somatosensory body nociception from DRG to the PB<sub>L</sub>: DRG  $\rightarrow$  spinal dorsal horn  $\rightarrow$  PB<sub>L</sub>.

Notably, a previous study using TrpV1::PLAP mice observed that fibers from a possible primary afferent source of TrpV1-lineage neurons were present in the PB<sub>L</sub>, especially in the PB-el<sup>29,32</sup>. The authors speculated that the TrpV1<sup>+</sup> fibers may have emerged from TG neurons which could provide an alternative circuit contributing to craniofacial pain experience<sup>29,32</sup>. These previous findings, in addition to our finding that ~40% of transsynaptically labeled TG neurons are TrpV1<sup>+</sup>, led us to postulate that TrpV1<sup>+</sup> fibers may be a major source of noxious TG inputs to PB-el. Therefore, we performed neonatal intraperitoneal (IP) injection of AAV to selectively label periphery-derived TrpV1-Cre<sup>+</sup> axons<sup>33,34,35</sup>. Briefly, Cre-dependent AAV9-flex-GFP was injected into TrpV1-Cre<sup>+</sup> mouse pups at postnatal day 1–2. The IP injection resulted in selective labeling of TrpV1-Cre<sup>+</sup> primary sensory neurons with GFP without labeling of TrpV1-Cre<sup>+</sup> CNS neurons (Fig. 3r, s and Supplementary Fig. 4, n = 3). Furthermore, axonal terminals from labeled TrpV1<sup>+</sup> primary sensory neurons were observed near nociceptive Fos<sup>+</sup> neurons in PB-el and in Sp5C (Fig. 3t; Fos was induced by capsaicin injection into the ipsilateral whisker pad).

We further designed a TrpV1-Cre and retrograde-FlpO intersectional strategy (Supplementary Fig. 5a) to determine whether PB<sub>L</sub> projecting TG neurons also project to Sp5C. Briefly, retrograde-lentivirus expressing either FlpO (RG-LV-hSyn-FlpO, n=4) or Cre-dependent FlpO (RG-LV-hSyn-DIO-FlpO, n=6) was injected into PB in TrpV1-Cre; Ai65 mice (Supplementary Fig. 5a). Retrograde-lentivirus infects axons and is transported back to cell bodies<sup>36,37</sup>. Ai65 is a Cre and Flp co-dependent tomato reporter<sup>38</sup>. In this strategy, only TrpV1-Cre expressing neurons that project axons into PB will express both Cre and FlpO, and therefore only these neurons will express tomato, allowing us to visualize their cell bodies and axon projections. The Cre-dependent RG-LV-hSyn-DIO-FlpO gave sparser labeling results than the RG-LV-hSyn-FlpO. We observed tdTomato<sup>+</sup> neurons in ipsilateral TG (Supplementary Fig. 5c, f) but not in any DRG (data not shown). Interestingly, tdTomato<sup>+</sup> axons can be seen in both PB<sub>L</sub> and in Sp5C (Supplementary Fig. 5b, d, e, g), indicating that at least some of the labeled TG neurons project bifurcated axons to innervate both PB<sub>L</sub> and Sp5C. The peripheral axons of labeled TrpV1-Cre<sup>+</sup> TG  $\rightarrow$  PB<sub>L</sub> neurons form either free-nerve endings or circular endings around hair follicles (Supplementary Fig. 5h).

### TrpV1-Cre<sup>+</sup> primary trigeminal sensory neurons provide functional monosynaptic excitatory input onto PB<sub>L</sub>-pain neurons

To directly examine whether TG  $\rightarrow$  PB<sub>L</sub> axons form functional synaptic connections in PB<sub>L</sub>, we injected Cre-dependent AAV9-flex-ChR2-YFP into TrpV1-Cre pups intraperitoneally to express channelrhodopsin-YFP (ChR2-YFP) in peripheral TrpV1-Cre<sup>+</sup> neurons



(TrpV1Cre::ChR2), and performed whole-cell patch clamp recording of PB<sub>L</sub> neurons in slices from these animals (Fig. 4a). Photoactivation of TrpV1Cre::ChR2<sup>+</sup> terminals elicited excitatory post-synaptic currents (EPSCs) in 15 out of 54 neurons (Fig. 4b, c and Supplementary Fig. 6). Furthermore, the EPSCs persisted in the presence of action potential blockade using 1 μM TTX and 100 μM 4-AP (Fig. 4b). In a complementary set of experiments, we captured PB<sub>L</sub>-pain neurons using CANE-RV-mCherry in TrpV1Cre::ChR2 animals (Fig. 4d). In 6 CANE-captured mCherry<sup>+</sup> PB<sub>L</sub>-pain neurons, photoactivation of TrpV1<sup>+</sup> terminals elicited EPSCs that were not blocked by TTX (Fig. 4e, f). These results corroborate and extend the circuit tracing findings that the inputs from TG TrpV1-Cre<sup>+</sup> fibers to PB<sub>L</sub>-nociceptive neurons are monosynaptic and excitatory.

### **Activation of TrpV1-Cre<sup>+</sup> axon terminals in PB<sub>L</sub> induces robust aversive behavior and audible vocalization**

To address the behavioral impact of the direct TG→PB<sub>L</sub> monosynaptic projection in awake behaving animals, we asked whether its activation would be sufficient to elicit aversive responses in a modified real-time place escape/avoidance (PEA) assay, which has been used in recent studies to assay affective components of pain<sup>39-41</sup>. Optic fibers were implanted bilaterally above PB-el in either TrpV1Cre::ChR2 mice (n = 8) or control mice TrpV1Cre::GFP (n = 3) mice (Fig. 4g). Mice were habituated and placed in a two-chamber arena. Their behaviors were recorded under three conditions: (i) freely exploring with no stimulation for 10 min (baseline), followed by (ii) 10 min of conditioned photoactivation when the mouse is in its preferred chamber (stimulation), and followed again by (iii) 10 min without stimulation (post-stimulation). Upon photo stimulation of TrpV1Cre<sup>+</sup> axons in PB-el, TrpV1Cre::ChR2 mice immediately fled to the opposite chamber (Fig. 4h; Video 1), and subsequently they moved less and spent significantly more time on the un-stimulated side (Fig. 4h, j-k, Video 1; P < 0.0001). In the post-stimulation period, some but not all mice still showed avoidance of the chamber in which they received photostimulation (Fig. 4j-k). Light illumination had no effect on movement and behavior of the control TrpV1Cre::GFP mice (Fig. 4i, j, l; Video 2; P = 0.66). These results suggest that the optogenetic stimulation of the TG→PB<sub>L</sub> monosynaptic projection caused a drastic aversive effect likely due to activation of the downstream affective pain pathway.

We further wanted to determine whether optogenetic activation would be sufficient to induce an aversive affective memory using the conventional conditioned place aversion (CPA) assay (Supplementary Fig. 7a). Mice were habituated first by placing them in the two-chamber arena and allowing free exploration. Subsequently, they were subjected to two days of conditioning: mice were paired with photostimulation in the preferred chamber for 15 min and four hours later, they were placed in the non-preferred chamber with no stimulation for 15 min. On the fourth day, they explored the arena freely with no light stimulation for 10 min (post-stimulation). All TrpV1Cre::ChR2 mice (n = 7) spent less time in the chamber where they were stimulated previously (Supplementary Fig. 7b, c; P = 0.008). Light illumination had no effect on the movement and behavior of the control TrpV1Cre::GFP mice (n = 5; Supplementary Fig. 7d, e; P = 0.258). These results suggest that repeated optogenetic activation of the TG→PB<sub>L</sub> monosynaptic projection induces an aversive memory.

We further recorded audios of mice placed in a circular arena (Fig. 4m). Optogenetic activation of TrpV1-Cre<sup>+</sup> afferents in PB-el induced audible vocalizations in TrpV1Cre::ChR2 (n = 8) resembling distress calls, but not in control TrpV1Cre::GFP mice (n = 3) (Fig. 4n, Supplementary Fig. 8, Videos 3, 4, on average 66 ± 7 pips with 2 ± 0.2 pips/second were elicited; P < 0.0001). Distress vocalization stopped when laser light was turned off. Post-hoc immunostaining conducted after photo-stimulation of the TrpV1Cre::ChR2 axon terminals in the PB<sub>L</sub> showed marked Fos expression in this region, whereas only background Fos expression was observed in Sp5C (Supplementary Fig. 9a, b), indicating that there was little back propagation of activities from PB<sub>L</sub> axon-terminal photo-stimulation to the axon branches of TG sensory neurons in Sp5C. Post-hoc immunostaining after photo-stimulating TrpV1Cre::GFP axon terminals only showed background level Fos expression (Supplementary Fig. 9c, n = 5). Taken together, these data demonstrate that activating the direct axonal projection from TrpV1-Cre<sup>+</sup> terminals in PB-el is sufficient to induce robust escape/avoidance behavior, aversive memory, and audible distress vocalizations, which are surrogates of pain behavior and pain-associated negative affect.

### **Silencing TrpV1-Cre<sup>+</sup> axon terminals in PB<sub>L</sub> partially reduces mechanical allodynia in face but not in hindpaw after capsaicin injection**

We next asked whether silencing the direct TG → PB<sub>L</sub> monosynaptic projection would affect pain-related behaviors. Previous studies showed that the optogenetic silencer archaerhodopsin (Arch) could effectively silence nociceptors including TrpV1+ neurons<sup>42,43</sup>. We therefore used the neonatal IP injection strategy to express eArch<sup>44</sup> or GFP in TrpV1-Cre<sup>+</sup> sensory neurons. Optic fibers were implanted bilaterally above PB-el in TrpV1Cre::eArch mice (n = 9) or TrpV1Cre::GFP (n = 8) mice (Fig. 5a, b). A von Frey test was used to assess the mechanical threshold of face or paw withdrawal responses before and after capsaicin injections into the whisker pad or hindpaw, and with or without photo-silencing of TrpV1-Cre<sup>+</sup> axons in PB<sub>L</sub> (Fig. 5a). After capsaicin injection into either the face or the paw, both TrpV1Cre::eArch and TrpV1Cre::GFP mice drastically lowered the withdrawal threshold in responses to von Frey application to face or paw, respectively (Fig. 5c, d). Hence, capsaicin-injection induced mechanical allodynia in both face and hindpaw as expected (Fig. 5c, d). Importantly, eArch-mediated photo-silencing of TrpV1-Cre<sup>+</sup> axons in PB-el partially alleviated the capsaicin induced allodynia in the face but had no effect on the mechanical hypersensitivity of the hindpaw (Fig. 5c, d; face P = 0.0046, paw P = >0.9999). Light illumination had no effect on TrpV1Cre::GFP mice (Fig. 5c, d; P = >0.9999). These results confirmed that the TG → PB<sub>L</sub> direct pathway indeed specifically contributes to face nociception.

We further tested whether photo-silencing of TrpV1-Cre<sup>+</sup> axons in PB<sub>L</sub> after facial capsaicin injection would elicit conditioned place preference for the light illuminated chamber. The effect of capsaicin only lasts about 20 min, we therefore performed a real-time place preference (RTPP) assay (Fig. 5e, 10 min no light and 10 min with light illumination in the non-preferred chamber). After capsaicin injection into the whisker pad, TrpV1Cre::eArch mice spent significantly more time in the chamber with photo-silencing of the TrpV1-Cre<sup>+</sup> terminals in PB<sub>L</sub> (Fig. 5f, n = 6, P = 0.029). By contrast, control TrpV1Cre::GFP mice show no preference (Fig. 5g, n = 7, P = 0.6). Taken together, these data demonstrated that when



mice are subjected to noxious facial stimulation, silencing the neural activity of the direct TG→PB<sub>L</sub> pathway reduces facial allodynia and induces place preference, indicating that this pathway contributes significantly to the manifestation of facial-pain equivalents.

## Discussion

In this study, we discovered that nociceptive trigeminal afferents transmit painful signal to the affective pathway through both the direct monosynaptic TG→PB<sub>L</sub> and the indirect disynaptic TG→Sp5C→PB<sub>L</sub> projections. Previously Panneton et al injected neural tracer WGA-HRP into the peripheral anterior ethmoidal nerve (AEN), which is originated from TG and innervate the nasal cavity, and observed labeled afferent fibers in regions near PB<sub>L</sub><sup>31</sup>. In a follow-up study, the authors showed that trigeminal rhizotomy resulted in loss of CGRP expressing fibers innervating the PB<sub>L</sub><sup>30</sup>. These and other studies have implied a possible direct TG→PB<sub>L</sub> pathway<sup>29–32</sup>, but did not provide synaptic or behavior evidence to support this possibility. Here we used a combination of activity-dependent tagging, monosynaptic transsynaptic tracing, intersectional genetic labeling, optogenetic-assisted slice electrophysiology, and in vivo optogenetic activation and silencing experiments to definitely establish the monosynaptic connection between TG and PB<sub>L</sub>-nociceptive neurons, and revealed the important functions of this pathway in craniofacial pain-related aversive behaviors.

Our findings have several important implications. First, the dual and bilateral pain-transmitting pathways compared to the single indirect DRG→dorsal horn→PB<sub>L</sub> pathway could explain why similar intensity stimuli applied to face activate more PB<sub>L</sub> neurons than when applied to limbs. This could in turn lead to heightened and bilateral activations of the affective pain responses, such as a higher level and more persistent activation of CeA, BNST, hypothalamus, and insular cortex through the axonal projections from PB<sub>L</sub>-nociceptive neurons (Fig. 2k-r). This projection pattern can provide a circuit basis for the perception of trigeminally-mediated pain as more severe, fear-inducing and emotionally-draining than other body pain. The monosynaptic TG→PB<sub>L</sub> connection also provides a mechanism for rapid, short-latency direct connections of nociceptive inputs from the head and face to brain centers involved in homeostatic regulation and emotional processing<sup>5,6,15,21,23,45</sup>. Second, current palliative neurosurgical procedures aimed at alleviating refractory trigeminal pain target the descending spinal trigeminal tract (Supplementary Fig. 10) including making thermal lesions, referred to as “dorsal root entry zone coagulation” (DREZ), to lesion pain-transmitting pathways in Sp5C, a contemporary adaptation of the classic trigeminal tractotomy<sup>46,47</sup>. Based on our study, DREZ coagulation will only lesion the TG→Sp5C connection, while leaving the TG→PB<sub>L</sub> connection intact (Supplementary Fig. 10). This may explain the lack of therapeutic response or post-operative pain relapse in some patients subjected to trigeminal DREZ surgery<sup>46–48</sup>. Future surgical procedures should consider severing both TG→Sp5C and the TG→PB<sub>L</sub> connection for providing invasive palliation of chronic, refractory orofacial pain, e.g. for trigeminal neuralgia. Notably, our discovery presented here critically relied on the CANE methodology, although CANE does have qualifiers, namely the 60~90min waiting interval between the stimulus application and the surgery (in order for Fos/TVA protein to reach peak levels) inevitably resulted in some background labeling. Nevertheless, CANE is still the most well-

validated tool to selectively label and transsynaptically trace the presynaptic inputs to transiently activated neurons as shown here and in our previous studies<sup>12</sup>. Our input-output circuit mapping of PB<sub>L</sub>-nociceptive neurons revealed many limbic centers that are reciprocally connected with PB<sub>L</sub>, providing a circuit basis for understanding closely associated and clinically highly-relevant comorbidities with pathologic trigeminal pain, namely anxiety, depression, disturbance of circadian rhythm and altered intake behavior<sup>2,3,47-50</sup>. Future studies on mechanisms underlying chronic craniofacial pain disorders can now take advantage of this circuit diagram including the newly unveiled monosynaptic TG→PB<sub>L</sub> pathway to identify specific maladaptive plasticity in each of the nodes in the circuit, and hopefully effectively revert them.

## Online Methods

### Animal Statement

All experiments were conducted according to protocols approved by The Duke University Institutional Animal Care and Use Committee.

### Animals

Adult (p30-p60) male and female C57B/L6 mice (Jackson Laboratory) were used for immunohistochemistry and in situ hybridization. Male and female Fos<sup>TVA</sup> mice<sup>12</sup> (Jackson Laboratory, stock 027831) were used for capturing PB<sub>L</sub>-nociceptive neurons with the CANE technology, immunohistochemistry, electrophysiology, and input-output circuit mapping. Male and female Ai65D<sup>38</sup> mice expressing a Cre and Flp double-dependent STOP cassette in front of the tdTomato reporter (Jackson Laboratories, stock 024109) were used for Cre/FlpO based tracing of TrpV1Cre<sup>+</sup> neurons that project to PB<sub>L</sub>. Male and Female TrpV1-Cre mice<sup>33</sup> were used for behavioral testing for both Chr2 or eArch experimental and GFP control groups, as well as electrophysiology experiments. Male and female Ai32 mice expressing a Cre-dependent Chr2 (Jackson Laboratories, stock 024109) were used for electrophysiology experiments. All mice were housed in a vivarium with normal light/dark cycles in cages with 1–5 mice. A day prior to experiments, we singly housed mice. We used two exclusion criteria for our subjects: (1) poor recovery or other health concerns following surgical intervention or (2) missed injection or implantation target, as determined by histological analysis. Animals were randomly selected from each litter. Random group allocation was maintained throughout the study, within constraints set by availability of in-house, purpose-bred lines. Experimenter blinding was sufficient to control for selection bias. Furthermore, behavioral analysis relied on objective, automatized measurements.

### Viruses

CANE-LV-Cre (titer,  $5 \times 10^8$  ifu/ml; pLenti-hSynapsin-Cre-WPRE [Addgene Plasmid #86641]; CANE-LV envelope [Addgene Plasmid #86666]) and CANE-RV-mCherry (titer,  $5 \times 10^8$  ifu/ml) were produced as previously described<sup>12</sup>. FuGB2-coated RG-LV-hSyn-FlpO and RG-LV-hSyn-DIO-FlpO were produced and concentrated as described previously<sup>36</sup>. pAAV-SynP-DIO-TVA-EGFP-RG (pAAV-SynP-DIO-sTpEpB)<sup>28</sup> was packaged in serotype AAV2/rh8 by the University of Pennsylvania Vector Core. AAV-CAG-flex-GFP, AAV-EF1 $\alpha$ -

flex-ChR2(H134R)-eYFP<sup>51</sup> and AAV-EF1 $\alpha$ -DIO-eARCH-eYFP<sup>44</sup> were purchased from the University of Pennsylvania Vector Core.

## Surgery

Animals were anesthetized with isoflurane in a stereotaxic frame (David Kopf Instruments) and small craniotomies were made over the target area. To target the PB<sub>L</sub>, mice were mounted in the stereotaxic frame at an angle such that lambda was ~180  $\mu$ m ventral to bregma (in practice, 140–240  $\mu$ m). The stereotaxic coordinates of virus injection and custom-made optic fiber (200  $\mu$ m core diameter, Thorlabs) were AP - 4.25  $\pm$  .15 mm, ML 1.45  $\pm$  .15 mm, and DV -3.2  $\pm$  .1 mm. The thin glass capillary was slowly lowered to the target site to minimize the brain injury. Virus was delivered into the target site at a flow rate of 100 nl per min using a pulled thin glass capillary (Warner Instruments) connected to an UltraMicroPump controlled by a SYS-Micro4 Controller 15 (World Precision Instruments).

For transsynaptically labeling experiment, CANE-LV-Cre and AAV-SynP-DIO-TVA-EGFP-RG were co-injected in animals subjected to 4% formalin injection; injected animals were singly housed for 2 weeks followed by CANE-RV-mCherry injection. For retrograde labeling experiment, RG-LV-hSyn-FlpO or RG-LV-hSyn-DIO-FlpO were injected in TrpV1Cre::Ai65D animals.

For neonatal intraperitoneal (IP) injections, postnatal day 1–2 pups were anesthetized with hyperthermia. 6 weeks after neonatal IP injection, mice were subjected to bilateral implantation of a custom-made optic fiber. After another 1~2 weeks of recovery, implanted animals were subjected to behavioral testing.

The injected viruses and the waiting period for viral transgene expression for the different experiments are: for experiments in Figure 2, CANE-LV-Cre (500 nl) together with AAV-CAG-flex-GFP (300 nl), waiting >10 days or > 4 weeks; for experiments in Figure 3(a-o), CANE-LV-Cre (500 nl) together with AAV-SynP-DIO-TVA-EGFP-RG (200 nl), waiting 2 weeks, then CANE-RV-mCherry (1:200 dilution, 300 nl), waiting additional 10 days; for experiment in Figure 4(d-f), CANE-RV-mCherry (1:200 dilution, 300 nl), waiting 3 days. For experiments in Figure 3(r-t) & 4(a-c, g-m), AAV9-CAG-flex-GFP (5  $\mu$ L) or AAV9-EF1 $\alpha$ -DIO-hChR2-eYFP (5  $\mu$ L), waiting 4–6 weeks. For experiments in Figure 5, AAV9-EF1 $\alpha$ -DIO-eArch-eYFP (8  $\mu$ L), waiting 4–6 weeks. For experiments in Supplemental Figure 5, RG-LV-h-Syn-DIO-FlpO or RG-LV-hSyn-FlpO (800 nL), waiting 3 weeks.

## Immunohistochemistry

All mice were deeply anaesthetized with isoflurane, and then transcardially perfused with ice-cold 4% paraformaldehyde in 0.1 M phosphate buffer, pH 7.4 (4% PFA). Dissected brain samples were then post-fixed overnight in 4% PFA at 4  $^{\circ}$ C, cryoprotected in a 20% sucrose solution in PBS at 4  $^{\circ}$ C, frozen in Tissue-Tek O.C.T. Compound (Sakura) and stored at -80  $^{\circ}$ C until sectioning. Trigeminal and dorsal root ganglion samples were sliced at 20  $\mu$ m using a cryostat (Leica Biosystems). All other coronal brain sections were sliced at 60–80  $\mu$ m. The serial brain sections were collected in a 24 well plate and washed with PBS for 3 times. The sections were blocked with 2% bovine serum albumin (BSA) in PBS with 0.3% Triton X-100 (Blocking solution) at room temperature for 1 h. The sections were treated

with 1st antibody in blocking solution at 4°C for overnight. The sections were washed 3 times followed by secondary antibody treatment at 4°C for 2 hours. Sections were counter stained NeuroTrace fluorescent Nissl stain (fluorescent Nissl stain) (Invitrogen, N-21479) or 4', 6-diamidino-2-phenylindole (DAPI) (Sigma, D9564). After this incubation, sections were washed, mounted and coverslipped. The primary antibodies used in this study are: goat anti-Fos<sup>12</sup> (Santa Cruz Biotechnology, sc52-g, 1:300), rabbit anti-CGRP<sup>52</sup> (Millipore, AB15360, 1:1000), sheep anti-FoxP2<sup>17</sup> (R&D Systems, AF5647, 1:5000), rabbit anti-NF200<sup>53</sup> (Sigma, N4142, 1:200), GS-IB4-Alexa 488–conjugated (Invitrogen, I21411, 1:1000), rabbit anti-VR1(TrpV1)<sup>54</sup> (Abcam, ab31895, 1:1000), and rabbit anti-GFP<sup>12</sup> (Abcam, ab290, 1:1000). The secondary antibodies are: Alexa Fluor 488 donkey anti-goat (Jackson immunoresearch, 705-545-147 1:1,000), Cy3 donkey anti-goat (Jackson immunoresearch, 705-165-147, 1:1,000), Alexa Fluor 488 donkey anti-rabbit (Jackson immunoresearch, 703-545-155, 1:1,000), Cy3 donkey anti-rabbit (Jackson immunoresearch, 711-165-152, 1:1,000), and Alexa Fluor 488 donkey anti-sheep (Abcam, ab150181, 1:1000)

### Floating section in situ hybridization

For each mouse, six 60 µm sections containing the PB<sub>L</sub> were collected and in situ was performed as described previously<sup>36</sup>. *Gad1*, *Gad2*, *vGlut2* and *Fos* probes were created as previously described<sup>12,37</sup>, and *Gad1* and *Gad2* probes were applied as a mixed probe. The probes were alternated across all sections to ensure that one posterior section and one anterior section from each region was analyzed with each probe type.

### Image Acquisition and Quantification

Samples were imaged using a Zeiss 700 laser scanning confocal microscope. *In situ* samples were imaged at 20× resolution at three *z*-positions. All *z*-positions for each slice were merged into a single image in Adobe Photoshop CS6 for quantification. All other samples were imaged at 10× resolution. The captured neurons and Fos expressing neurons in all immunohistochemistry and *in situ* hybridization experiments were manually counted, and percentages were calculated within each animal before averaging percentages across animals.

Axonal projections from captured PB<sub>L</sub>-nociceptive neurons was quantified using a method previously described<sup>12, 28</sup>. The projection density for ROI's was quantified across every other 80 µm coronal section. The data was normalized between animals by their own values in CeA (Central Amygdala). ROI's with densities in which the total pixel numbers of GFP-labeled axons divided by the area of the nuclei was less than 0.1 were excluded.

Again, using a method previously described<sup>12</sup>, the number of transsynaptically labeled neurons from captured PB<sub>L</sub>-nociceptive neurons was quantified across every other 80 µm coronal section. Numbers of labeled cells in each ROI were manually counted. The data was normalized between animals by dividing with the number of starter neurons (GFP and mCherry double positive neurons in the PB<sub>L</sub>) in each animal.

### Behavioral experiments for Fos immunostaining

Adult male and female C57B/L6 mice at ages more than 6 weeks were singly housed at least one day before noxious stimulation. Singly housed mice were directly perfused to stain for background Fos expression. For visualizing Fos expression induced by nociceptive stimuli, mice were lightly anesthetized with isoflurane, and unilaterally injected with 10  $\mu$ L of saline, or 4% capsaicin, or 4% formalin into either the whisker pad or the hindpaw and returned to their home cage. 90 minutes later, the animals were perfused (as described in the method for immunostaining above).

### Behavioral experiments for capturing PB<sub>L</sub>-nociceptive neurons with CANE virus

A brief description of CANE method: in Fos<sup>TVA</sup> mice, activated neurons transiently express Fos which induces expression of a destabilized TVA (dsTVA) receptor. Lentivirus or deficient rabies virus pseudotyped with an engineered mutated envelope protein (CANE envelope) specifically binds cells expressing high-level TVA receptor, which are strongly Fos<sup>+</sup> neurons. In this way, CANE-viruses selectively infect Fos<sup>+</sup> neurons and deliver desired transgenes to be expressed in Fos<sup>+</sup> neurons.

Here, adult male and female Fos<sup>TVA</sup> mice at ages more than 6 weeks were singly housed for at least one day, and then either handled without injection, or handled and subjected to noxious stimulation. Briefly, mice were taken out of their home cage, placed in the anesthesia chamber, lightly anesthetized with isoflurane, and injected unilaterally with 10  $\mu$ L of saline or 4% capsaicin or 4% formalin into either the whisker pad or the hindpaw, and returned to their home cage. 60–90min later, mice were anesthetized and undergo stereotaxic surgery for CANE-virus injection. Note that PB is a relatively large area and formalin/capsaicin activated neurons spread along both the dorsal-ventral as well as anterior-posterior axes; while we only injected CANE virus once using one stereotaxic coordinate, so we could only capture some of the neurons. Additionally, injections of formalin/capsaicin in whisker pad on different days could not hit the identical site, and this likely resulted in activation (Fos<sup>+</sup>) of overlap but none-identical populations of PB neurons.

### Electrophysiological recording in acute brainstem slices

Four weeks after intraperitoneal injection of AAV9-EF1a-flex-ChR2-eYFP into TrpV1-Cre P1-2 mice, or 3 days after injection of CANE-RV-mCherry into the PB<sub>L</sub> of TrpV1-Cre::Ai32;Fos<sup>TVA</sup> mice, mice were anesthetized with isoflurane, and transcatheterially perfused in ice-cold NMDG artificial cerebrospinal fluid (NMDG-ACSF; containing 92 mM NMDG, 2.5 mM KCl, 1.2 mM NaH<sub>2</sub>PO<sub>4</sub>, 30 mM NaHCO<sub>3</sub>, 20 mM HEPES, 2 mM glucose, 5 mM sodium ascorbate, 2 mM thiourea, 3 mM sodium pyruvate, 10 mM MgSO<sub>4</sub>, 0.5 mM CaCl<sub>2</sub>), and bubbled with 5% CO<sub>2</sub> / 95% O<sub>2</sub>. The brain was then extracted and sectioned into 250  $\mu$ m thick sagittal slices using a vibratome (VT-1000S, Leica Microsystems) containing ice-cold oxygenated NMDG-ACSF. Sagittal sections including the PB<sub>L</sub> were then bubbled in same solution at 37 °C for 8 min, and transferred to bubbled, modified-HEPES ACSF at room temperature (20–25 °C; 92 mM NaCl, 2.5 mM KCl, 1.2 mM NaH<sub>2</sub>PO<sub>4</sub>, 30 mM NaHCO<sub>3</sub>, 20 mM HEPES, 2 mM glucose, 5 mM sodium ascorbate, 2 mM thiourea, 3 mM sodium pyruvate, 2 mM MgSO<sub>4</sub>, 2 mM CaCl<sub>2</sub>) for at least 1 h before recording. Recordings were performed in a submerged chamber, superfused with

continuously bubbled ACSF (125 mM NaCl, 2.5 mM KCl, 1.25 mM NaH<sub>2</sub>PO<sub>4</sub>, 26 mM NaHCO<sub>3</sub>, 20 mM glucose, 2 mM CaCl<sub>2</sub>, 1.3 mM MgSO<sub>4</sub>) at near-physiological temperature (34 ± 1°C). Cells expressing GFP were visualized by infrared differential interference contrast and fluorescence video microscopy (Examiner.D1, Zeiss). Whole-cell current clamp recordings were amplified with Multiclamp 700B (filtered at 2 kHz), digitized with Digidata 1440A (5 kHz), and recorded using pClamp 10 software (Axon). Both unlabeled and mCherry<sup>+</sup> PB<sub>L</sub> cells surrounded by axon terminals expressing a virally encoded fluorescent marker (ChR2-EYFP) were visualized by infrared differential interference contrast and fluorescence video microscopy (Examiner.D1, Zeiss). Whole-cell voltage-clamp recordings were amplified with Multiclamp 700B (filtered at 2 kHz), digitized with Digidata 1440A (5 kHz), and recorded using pClamp 10 software (Axon). The patch-clamp electrode (4–6 MΩ) was filled with an intracellular solution containing 130 mM D-gluconic acid, 130 mM CsOH, 5 mM NaCl, 10 mM HEPES, 12 mM phosphocreatine, 3 mM MgATP, 0.2 mM Na<sub>2</sub>GTP, 1 mM EGTA. Photostimulation was performed using a 473 nm LED (CoolLED, pE4000) controlled by pClamp 10 software (Axon). Light intensity was set to be 100% for generation of spikes in the axon terminals of projecting TrpV1Cre::ChR2<sup>+</sup> neurons with a pulse length of 10 ms. To confirm whether post-synaptic currents were monosynaptic, tetrodotoxin (TTX; 1 μM) was initially bath applied, followed by a combination of TTX and 4-aminopyridine (4-AP; 100 μM).

All electrophysiology data were analyzed off-line using Neuromatic package (Think Random) in Igor Pro software (WaveMetrics). Off-line analysis was performed by averaging five traces. Light-evoked EPSC and IPSC peak amplitude, half-width, onset latency, time to peak, rise time, and decay time were analyzed. The onset latency of the light-evoked EPSCs and IPSCs was defined as the time from the onset of the stimulus to the first measurable deflection of the potential from the baseline. Similarly, time to peak was defined as the time from the onset of the stimulus to the peak of the potential. Rise time and decay time were defined as the time between 10% and 90% of the rise or decay of the potential, respectively.

### **Optogenetic activation of TrpV1Cre::ChR2<sup>+</sup> sensory afferent terminals in PB<sub>L</sub> in a real-time place escape/avoidance (PEA) test and in circular chamber for audio recording**

Channelrhodopsin (ChR2) or control GFP was expressed in TrpV1-Cre<sup>+</sup> primary sensory neurons by neonatal IP injection of either AAV9-EF1α-DIO-hChR2-eYFP or AAV9-CAG-Flex-GFP in TrpV1-Cre pups (as described above). Six weeks later, virus injected mice were implanted with custom-made optic fibers which were placed above PB-el on both sides and fixed on the skull with dental cement (Parkell). One week later, the animals were subjected to a 2-chamber real-time PEA test in light cycle, using a modified method described previously<sup>55,56</sup>. The size of custom-made behavior chamber is 50.1×27.7×31.2 cm, made with clear acrylic Plexiglas that had distinct stripe patterns from one another. For optogenetic stimulation, laser is delivered through patch cables attached to the implanted optic fiber as described previously<sup>12</sup>. The mouse is placed in the center of the box and allowed to explore both chambers without light stimulation (pre-stimulation) for 10 min. Generally, after exploration, the mouse shows a small preference for one of the two chambers. Subsequently, blue light stimulation (10 Hz, 20 ms pulse-width, ~3.5 mW) is delivered whenever the mouse enters or stays in the preferred chamber, and light is turned



OFF when the mouse moves to the other chamber (stimulation phase, total 10 min). Finally, the mouse can freely explore both chambers without blue light stimulation (post-stimulation) for 10 min. We recorded behavioral data via a webcam (Logitech web-camera, PN 960-000764) interfaced with Bonsai software<sup>57</sup>. Real-time laser stimulation was controlled by Bonsai software through Arduino with a custom-made Arduino sketch (Arduino UNO, A00073). After 1 week, the same group of mice were subjected to another behavioral test, where the mouse was placed in a circular field in a sound proof chamber. The mouse's movements and audible vocalizations were recorded from the top of field using the webcam with audio control at a frame rate 30 fps. The experimental mouse was placed in the center of the circular field and allowed to explore freely. Blue light was delivered as described above. The duration of each light stimulation was 30 s and the interval between light stimuli was > 2 min. The number of light stimulation for each mouse in each behavioral test was 4. The number of pips was calculated for each interval and averaged offline.

After all behavior tests were completed, the mice were given a train of strong light stimulations (15s on and 15 s off, 50 ms pulses, 10 Hz, ~3.5 mW, repeated 3 times) to elicit ChR2- or photo stimulation-dependent Fos expression in their home cage. Subsequently, animals were perfused at 90 minutes after the final stimulation and processed for Fos immunostaining.

#### **Optogenetic activation of TrpV1Cre::ChR2<sup>+</sup> sensory afferent terminals in PB<sub>L</sub> in a classical conditioned place aversion (CPA) test**

Channelrhodopsin (ChR2) or control GFP was expressed in TrpV1-Cre<sup>+</sup> primary sensory by neonatal IP injection of either AAV9-EF1 $\alpha$ -DIO-hChR2-eYFP or AAV9-CAG-Flex-GFP in TrpV1-Cre pups (as described above). Six weeks later, virus injected mice were implanted with custom-made optic fibers which were placed above PB-el on both sides and fixed on the skull with dental cement (Parkell). One week later, the animals were subjected to a 2-chamber classic conditioned place aversion (CPA) test in same behavior chamber used for PEA. The mouse is first habituated to the chamber on day 1. On day 2, the mouse is placed in the center of the box and allowed to explore both chambers without light stimulation (pre-stimulation) for 10 min. Generally, after exploration, the mouse shows a small preference for one of the two chambers. In the following two days (day 3 and day 4), the mouse is closed off in the non-preferred chamber with no stimulation for 15 min in the morning, and then closed off in the preferred chamber with blue light stimulation (10 Hz, 20 ms pulse-width, ~3.5 mW) for 15 min in the afternoon. On the final day (day 5), the mouse can explore both chambers without blue light stimulation (post-stimulation) for 10 min, and their behaviors are recorded and analyzed.

#### **Optogenetic silencing of TrpV1Cre::eArch<sup>+</sup> sensory afferent terminals in PB<sub>L</sub> in von Frey tests and real-time place preference (RTPP) test**

Enhanced archaerhodopsin (eArch) or control GFP was expressed in TrpV1-Cre<sup>+</sup> primary sensory by neonatal IP injection of either AAV9-EF1 $\alpha$ -DIO-eARCH-eYFP or AAV9-CAG-Flex-GFP in TrpV1-Cre pups (as described above). Six weeks later, virus injected mice were implanted with custom-made optic fibers which were placed above PB-el on both sides and fixed on the skull with dental cement (Parkell). More than one week later, the animals were

subjected to von Frey tests. All mice were first habituated to handling and testing equipment at least 30 min before experiments. Behavioral responses to mechanical stimuli applied to face or hindpaw at baseline (without capsaicin injection) were examined first and both in the absence and in the presence of photo illumination. Subsequently, capsaicin (Sigma-Aldrich, 1 $\mu$ g/10 $\mu$ l, dissolved in normal saline with 4% ethanol and 4% tween-80) was subcutaneously injected into either right hindpaw or right whisker pad. Between 10 and 20 min after capsaicin injection, behavioral responses to mechanical stimuli were tested either in the absence or the presence of photo-silencing/illuminating of TrpV1-Cre<sup>+</sup> axons in PB<sub>L</sub>. The mice were tested for hindpaw and face responses on different days with a randomized order (i.e. some were tested for face first, others were tested for paw responses first). There was at least one week interval separating the paw versus face (or vice versa) tests. For the hindpaw test, mice were individually placed on an elevated metallic wire mesh floor in polyethylene cages (4x4x5.5 inch, Comerio-VA, Italy). A graded series of von Frey filaments (0.04–2g, Stoelting) was inserted through the mesh floor and applied to the plantar surface of the hindpaw. For face test, mice were individually placed in a custom-made box (3x3x4 inch) with the top, bottom and four walls made of silver wire mesh and allowed for free movement. Again, a graded series of von Frey filaments (0.02–1g) was inserted through the mesh wells from the lateral side and applied to the skin of the vibrissa pad within the infraorbital nerve territory. A brisk withdrawal of the paw or head was considered a positive response. Mice were tested 3 times with at least 2 withdrawal behaviors out of 3 trials indicated a positive result. Mechanical threshold was defined as the minimum force necessary to elicit a response<sup>58–61</sup>. For optogenetic silencing during von Frey tests, a continuous green light (561nm) stimulation (~12 mW) was delivered during both the hindpaw and face tests (with and without capsaicin injections). Again, mice were tested 3 times with at least 2 withdrawal behaviors out of 3 trials indicated a positive result. Mechanical threshold was defined as the minimum force necessary to elicit a response.

TrpV1Cre::eArch and TrpV1Cre::GFP mice were also subjected to a real-time place preference test (RTPP). Individual mouse was placed in the center of the box and allowed to explore both chambers without light stimulation (baseline) for 10 min. Generally, after exploration, the mouse shows a small preference for one of the two chambers. After recording the baseline behavior, individual mouse was injected with 5 $\mu$ l 4% capsaicin into the left whisker pad and placed in the chamber again to freely explore both chambers without light stimulation (no stimulation) for 10 min again. Subsequently, a continuous green light stimulation (561 nm, ~12 mW) was delivered through the optic fiber to silence the TrpV1Cre::eArch<sup>+</sup> fibers (or illuminate the control GFP<sup>+</sup> fibers) in PB<sub>L</sub> whenever the mouse entered or stayed in the non-preferred chamber, and light was turned OFF when the mouse moved to the other chamber (total 10 min of real-time stimulation). We recorded behavioral data via a webcam (Logitech web-camera, PN 960-000764) interfaced with Bonsai software<sup>57</sup>. Real-time laser stimulation was controlled by Bonsai software through Arduino with a custom-made Arduino sketch (Arduino UNO, A00073). Matlab codes for controlling laser and triggering stimulation are available upon request. Subsequently, animals were perfused for post-hoc analysis.

## Statistics

No statistical methods were used to predetermine sample sizes, but our sample sizes are similar to those reported in previous publications<sup>12,62,63</sup>. Values in text are reported as mean  $\pm$  standard error of mean. All data (with the exception of behavioral data for the real-time PEA test) were analyzed using two-tailed paired and unpaired Student's *t* test between 2 groups (experimental or control), or in the case of multiple groups, one-way or two-way ANOVA followed by Tukey's test. The criterion for statistical significance was  $P < 0.05$ . Regarding the assumption of normality for large/medium data sets, D'Agostino and Pearson normality test was used. When the sample size was less than four, Shapiro-Wilk normality test was used. We provided mean values with associated standard error of the mean values. To determine whether the variance was similar between the groups that are being statistically compared, *F* test was used for *t* tests, and Brown-Forsythe was used for one-way ANOVA. The results showed that the variance was similar.

Behavioral data for real-time PEA and RTPP tests were analyzed using one-way repeated measures ANOVA with Matlab R2016a. The statistical test was used for ChR2 group and GFP group independently. For PEA, the preference of the stimulation side between PRE (no-stim), STIM, and POST (no-stim) periods was compared. For RTPP, the preference of the stimulation side between Baseline, No Stimulation, and Stimulation periods was compared. Tukey's test was used post-hoc. Behavioral data for von Frey tests were analyzed using two-way repeated measures ANOVA. The statistical test was used for face test and hindpaw test independently. For both tests, both between and within eArch and GFP groups was across conditions were compared.

A detailed Life Sciences Reporting Summary is available.

## Data availability

The data collected in this study are available from the corresponding author upon request.

## Code availability

All custom-written MatLab code used in this study is available at <https://github.com/wanglab-duke/craniofacial-specific-monosynaptic-circuit-for-affective-pain>

## Supplementary Material

Refer to Web version on PubMed Central for supplementary material.

## Acknowledgments

We thank J. Takatoh for helping with method to quantify axon innervation densities, K. Tschida and T. Gibson for helping with vocalization quantification and analysis, V. Prevosto for helping with statistics. We also thank T. Gibson, M. Fu, K. Tschida, T. Stanek, V. Prevosto, and R.R. Ji for providing input and support throughout the project. We also thank S. Lisberger, and R. Mooney for critically reading of this manuscript. E. Rodriguez. is supported by a F31 DE025197-03 fellowship. Y. Chen. is supported by K12DE022793. W. Liedtke is supported by DE018549. This work is supported by NIH Grant DP1MH103908 to F.Wang.

## References

1. Waldman, SD. Atlas of common pain syndromes. Elsevier Health Sciences; 2011.
2. Zakrzewska JM, Wu J, Williams MM, Phillips N, Pavitt SH. Evaluating the impact of trigeminal neuralgia. *Pain*. 2017
3. Smith JG, et al. The psychosocial and affective burden of posttraumatic neuropathy following injuries to the trigeminal nerve. *Journal of orofacial pain*. 2013; 27:293–303. [PubMed: 24171179]
4. Schmidt K, Schunke O, Forkmann K, Bingel U. Enhanced Short-Term Sensitization of Facial Compared With Limb Heat Pain. *The Journal of Pain*. 2015; 16:781–790. [PubMed: 26043953]
5. Schmidt K, et al. The differential effect of trigeminal vs. peripheral pain stimulation on visual processing and memory encoding is influenced by pain-related fear. *NeuroImage*. 2016; 134:386–395. [PubMed: 27015710]
6. Moulton EA, et al. Capsaicin-induced thermal hyperalgesia and sensitization in the human trigeminal nociceptive pathway: An fMRI study. *NeuroImage*. 2007; 35:1586–1600. [PubMed: 17407825]
7. Hunt SP, Mantyh PW. The molecular dynamics of pain control. *Nature reviews. Neuroscience*. 2001; 2:83–91. [PubMed: 11252998]
8. Gauriau C, Bernard J-FF. Pain pathways and parabrachial circuits in the rat. *Experimental physiology*. 2002; 87:251–258. [PubMed: 11856971]
9. Craig AD. Distribution of brainstem projections from spinal lamina I neurons in the cat and the monkey. *The Journal of comparative neurology*. 1995; 361:225–248. [PubMed: 8543660]
10. Hermanson O, Blomqvist A. Subnuclear localization of FOS-like immunoreactivity in the rat parabrachial nucleus after nociceptive stimulation. *The Journal of comparative neurology*. 1996; 368:45–56. [PubMed: 8725293]
11. Hermanson O, Blomqvist A. Subnuclear localization of FOS-like immunoreactivity in the parabrachial nucleus after orofacial nociceptive stimulation of the awake rat. *The Journal of comparative neurology*. 1997; 387:114–123. [PubMed: 9331175]
12. Sakurai K, et al. Capturing and Manipulating Activated Neuronal Ensembles with CANE Delineates a Hypothalamic Social-Fear Circuit. *Neuron*. 2016; 92:739–753. [PubMed: 27974160]
13. Slugg RM, Light AR. Spinal cord and trigeminal projections to the pontine parabrachial region in the rat as demonstrated with Phaseolus vulgaris leucoagglutinin. *The Journal of comparative neurology*. 1994; 339:49–61. [PubMed: 8106661]
14. Cechetto DF, Standaert DG, Saper CB. Spinal and trigeminal dorsal horn projections to the parabrachial nucleus in the rat. *Journal of Comparative Neurology*. 1985; 240:153–160. [PubMed: 3840498]
15. Han S, Soleiman MT, Soden ME, Zweifel LS, Palmiter RD. Elucidating an Affective Pain Circuit that Creates a Threat Memory. *Cell*. 2015; 162:363–374. [PubMed: 26186190]
16. Gaub S, Fisher SE, Ehret G. Ultrasonic vocalizations of adult male Foxp2 mutant mice: behavioral contexts of arousal and emotion. *Genes, Brain and Behavior*. 2016; 15:243–259.
17. Geerling JC, et al. FoxP2 expression defines dorsolateral pontine neurons activated by sodium deprivation. *Brain research*. 2011; 1375:19–27. [PubMed: 21108936]
18. Ding YQ, Takada M, Shigemoto R, Mizuno N. Trigemino-parabrachial projection neurons showing substance P receptor-like immunoreactivity in the rat. *Neuroscience research*. 1995; 23:415–418. [PubMed: 8602281]
19. Tokita K, Inoue T, Boughter JD. Afferent connections of the parabrachial nucleus in C57BL/6J mice. *Neuroscience*. 2009; 161:475–488. [PubMed: 19327389]
20. Nishijo H, Norgren R. Parabrachial neural coding of taste stimuli in awake rats. *Journal of neurophysiology*. 1997; 78:2254–2268. [PubMed: 9356379]
21. Nakamura K, Morrison SF. A thermosensory pathway that controls body temperature. *Nature Neuroscience*. 2007; 11:62–71. [PubMed: 18084288]
22. Alhadeff AL, Golub D, Hayes MR, Grill HJ. Peptide YY signaling in the lateral parabrachial nucleus increases food intake through the Y1 receptor. *American journal of physiology. Endocrinology and metabolism*. 2015; 309:66.

23. Davern PJ. A role for the lateral parabrachial nucleus in cardiovascular function and fluid homeostasis. *Frontiers in physiology*. 2014; 5:436. [PubMed: 25477821]
24. Menani JV, De Luca LA, Johnson AK. Role of the lateral parabrachial nucleus in the control of sodium appetite. *American journal of physiology. Regulatory, integrative and comparative physiology*. 2014; 306:10.
25. Bester H, Menendez L, Besson JM, Bernard JF. Spino (trigemino) parabrachiohypothalamic pathway: electrophysiological evidence for an involvement in pain processes. *Journal of neurophysiology*. 1995; 73:568–585. [PubMed: 7760119]
26. Bernard JF, Besson JM. The spino(trigemino)pontoamygdaloid pathway: electrophysiological evidence for an involvement in pain processes. *Journal of neurophysiology*. 1990; 63:473–490. [PubMed: 2329357]
27. Oh SW, et al. A mesoscale connectome of the mouse brain. *Nature*. 2014; 508:207–214. [PubMed: 24695228]
28. Kohara K, et al. Cell type-specific genetic and optogenetic tools reveal hippocampal CA2 circuits. *Nature Neuroscience*. 2014; 17:269–279. [PubMed: 24336151]
29. Cavanaugh DJ, et al. Restriction of transient receptor potential vanilloid-1 to the peptidergic subset of primary afferent neurons follows its developmental downregulation in nonpeptidergic neurons. *J Neurosci*. 2011; 31:10119–10127. [PubMed: 21752988]
30. Panneton WM, Gan Q. Direct reticular projections of trigeminal sensory fibers immunoreactive to CGRP: potential monosynaptic somatoautonomic projections. *Front Neurosci*. 2014; 8:136. [PubMed: 24926231]
31. Panneton WM, Gan Q, Juric R. Brainstem projections from recipient zones of the anterior ethmoidal nerve in the medullary dorsal horn. *Neuroscience*. 2006; 141:889–906. [PubMed: 16753263]
32. Cavanaugh DJ, et al. Trpv1 reporter mice reveal highly restricted brain distribution and functional expression in arteriolar smooth muscle cells. *J Neurosci*. 2011; 31:5067–5077. [PubMed: 21451044]
33. Mishra SK, Tisel SM, Orestes P, Bhargoo SK, Hoon MA. TRPV1-lineage neurons are required for thermal sensation. *The EMBO Journal*. 2011; 30:582–593. [PubMed: 21139565]
34. Foust KD, Poirier A, Pacak CA, Mandel RJ. Neonatal intraperitoneal or intravenous injections of recombinant adeno-associated virus type 8 transduce dorsal root ganglia and lower motor neurons. *Human gene therapy*. 2008; 19:61–70. [PubMed: 18052722]
35. Machida A, et al. Intraperitoneal administration of AAV9-shRNA inhibits target gene expression in the dorsal root ganglia of neonatal mice. *Molecular Pain*. 2013; 9:1–10. [PubMed: 23279936]
36. Stanek E, Rodriguez E, Zhao S, Han B-XX, Wang F. Supratrigeminal Bilaterally Projecting Neurons Maintain Basal Tone and Enable Bilateral Phasic Activation of Jaw-Closing Muscles. *J Neurosci*. 2016; 36:7663–7675. [PubMed: 27445144]
37. Bellavance MA, et al. Parallel Inhibitory and Excitatory Trigemino-Facial Feedback Circuitry for Reflexive Vibrissa Movement. *Neuron*. 2017; 95:673–682. [PubMed: 28735746]
38. Madisen L, et al. Transgenic mice for intersectional targeting of neural sensors and effectors with high specificity and performance. *Neuron*. 2015; 85:942–958. [PubMed: 25741722]
39. Baastrup C, Jensen T, Finnerup N. Pregabalin attenuates place escape/avoidance behavior in a rat model of spinal cord injury. *Brain research*. 2010; 1370:129–135. [PubMed: 21070753]
40. LaBuda CJ, Fuchs PN. A Behavioral Test Paradigm to Measure the Aversive Quality of Inflammatory and Neuropathic Pain in Rats. *Experimental Neurology*. 2000; 163:490–494. [PubMed: 10833324]
41. Zhang Z, et al. Role of Prelimbic GABAergic Circuits in Sensory and Emotional Aspects of Neuropathic Pain. *Cell Reports*. 2015; 12:752–759. [PubMed: 26212331]
42. Daou I, et al. Optogenetic Silencing of Nav1.8-Positive Afferents Alleviates Inflammatory and Neuropathic Pain. *eNeuro*. 2016; 3
43. Li B, et al. A novel analgesic approach to optogenetically and specifically inhibit pain transmission using TRPV1 promoter. *Brain Res*. 2015; 1609:12–20. [PubMed: 25797803]
44. Chow BY, et al. High-performance genetically targetable optical neural silencing by light-driven proton pumps. *Nature*. 2010; 463:98–102. [PubMed: 20054397]

45. Sato M, et al. The lateral parabrachial nucleus is actively involved in the acquisition of fear memory in mice. *Molecular Brain*. 2015; 8:1–15. [PubMed: 25571783]
46. Moffie D. Late results of bulbar trigeminal tractotomy Some remarks on recovery of sensibility. *Journal of Neurology, Neurosurgery & Psychiatry*. 1971; 34:270–274.
47. Rahimpour S, Lad SP. Surgical Options for Atypical Facial Pain Syndromes. *Neurosurgery clinics of North America*. 2016; 27:365–370. [PubMed: 27325003]
48. Romaniello A, Iannetti GD, Truini A, Cruccu G. Trigeminal responses to laser stimuli. *Neurophysiologie Clinique/Clinical Neurophysiology*. 2003; 33:315–324. [PubMed: 14678845]
49. DeSouza DD, Moayedi M, Chen DQ, Davis KD, Hodaie M. Sensorimotor and Pain Modulation Brain Abnormalities in Trigeminal Neuralgia: A Paroxysmal, Sensory-Triggered Neuropathic Pain. *PLoS ONE*. 2013; 8
50. Kuner R. Central mechanisms of pathological pain. *Nature Medicine*. 2010; 16:1258–1266.
51. Zhang F, et al. Optogenetic interrogation of neural circuits: technology for probing mammalian brain structures. *Nat. Protocols*. 2010; 5:439–456. [PubMed: 20203662]
52. Röhn TA, et al. A virus-like particle-based anti-nerve growth factor vaccine reduces inflammatory hyperalgesia: potential long-term therapy for chronic pain. *J Immunol*. 2011; 186:1769–80. [PubMed: 21191068]
53. Xu ZZ, et al. Inhibition of mechanical allodynia in neuropathic pain by TLR5-mediated A-fiber blockade. *Nature Medicine*. 2015; 21:1326–1331.
54. Koh WU, et al. Perineural pretreatment of bee venom attenuated the development of allodynia in the spinal nerve ligation injured neuropathic pain model; an experimental study. *BMC Complement Altern Med*. 2014; 14:431. [PubMed: 25366818]
55. Jennings JH, et al. Distinct extended amygdala circuits for divergent motivational states. *Nature*. 2013; 496:224–228. [PubMed: 23515155]
56. Stamatakis AM, Stuber GD. Activation of lateral habenula inputs to the ventral midbrain promotes behavioral avoidance. *Nature neuroscience*. 2012
57. Lopes G, et al. Bonsai: an event-based framework for processing and controlling data streams. *Frontiers in neuroinformatics*. 2015; 9:7. [PubMed: 25904861]
58. Silva JR, et al. Neuroimmune-Glia Interactions in the Sensory Ganglia Account for the Development of Acute Herpetic Neuralgia. *J Neurosci*. 2017; 37:6408–6422. [PubMed: 28576938]
59. Peng C, et al. miR-183 cluster scales mechanical pain sensitivity by regulating basal and neuropathic pain genes. *Science*. 2017; 356:1168–1171. [PubMed: 28572455]
60. Kim YS, et al. Central terminal sensitization of TRPV1 by descending serotonergic facilitation modulates chronic pain. *Neuron*. 2014; 81:873–887. [PubMed: 24462040]
61. Aita M, Byers MR, Chavkin C, Xu M. Trigeminal injury causes kappa opioid-dependent allodynic, glial and immune cell responses in mice. *Mol Pain*. 2010; 6:8. [PubMed: 20109235]
62. Zhang Y, et al. Identifying Local and Descending Inputs for Primary Sensory Neurons. *J Clin Invest*. 2015; 125:3782–3794. [PubMed: 26426077]
63. Zhang Y, Chen Y, Liedtke W, Wang F. Lack of evidence for ectopic sprouting of genetically labeled A $\beta$  touch afferents in inflammatory and neuropathic trigeminal pain. *Mol Pain*. 2015; 11:18. [PubMed: 25880319]



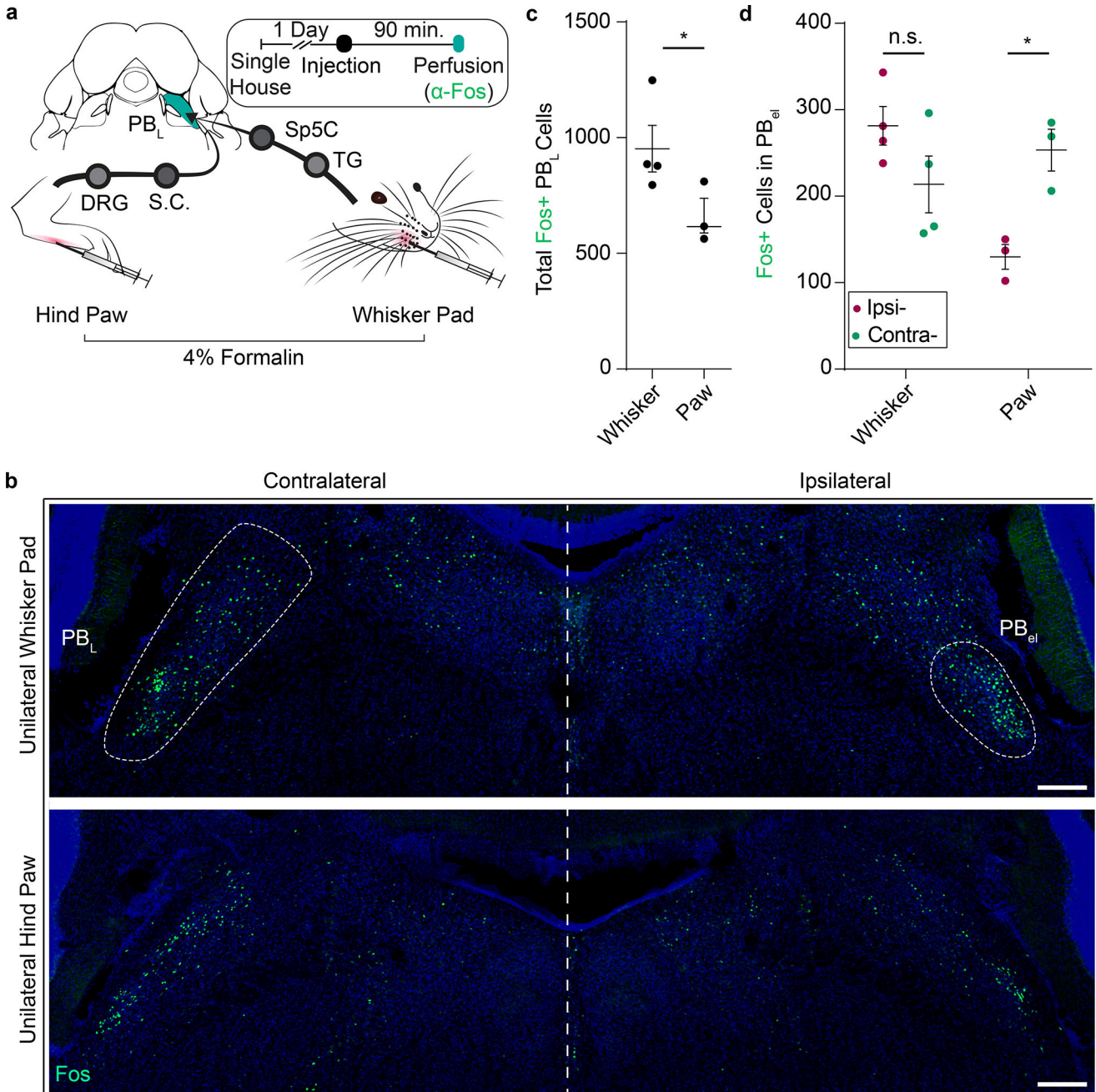


**Figure 1. Lateral parabrachial nucleus (PB<sub>L</sub>) is differentially activated by the same noxious stimulus applied to the face versus hindpaw**  
 (a) Schematic illustration of Fos induction protocol. Ninety minutes after 10 μL 4% formalin was injected, brainstem slices containing PB<sub>L</sub> were stained for Fos expression. (TG, trigeminal ganglion; Sp5C, trigeminal nucleus, caudalis; DRG, dorsal root ganglion; S.C., spinal cord)  
 (b) Representative images of Fos<sup>+</sup> neurons in PB<sub>L</sub> after formalin injection into right whisker pad (top) and right hindpaw (bottom). Large white dash circle (left) indicates the entire structure of PB<sub>L</sub>, whereas small white dash circle (right) indicates ventral region of PB<sub>L</sub> including PB-el. Blue; DAPI stain. Scale bar, 200 μm.

(c) Total numbers of Fos<sup>+</sup> neurons in PB<sub>L</sub> on both sides combined (n = 4, 3; two-tailed unpaired student's *t* test; \**P* = 0.0445;  $t_{4,962} = 2.674$ ).

(d) Numbers of Fos<sup>+</sup> neurons in ipsilateral (magenta) and contralateral (teal) PB-el in mice unilaterally injected with formalin into one whisker pad (n = 4) or one hindpaw (n = 3 mice; two-way ANOVA; W: *P* = 0.0533; H: \*\**P* = 0.0090;  $F_{1,5} = 32.75$ ). Data are mean ± SEM.

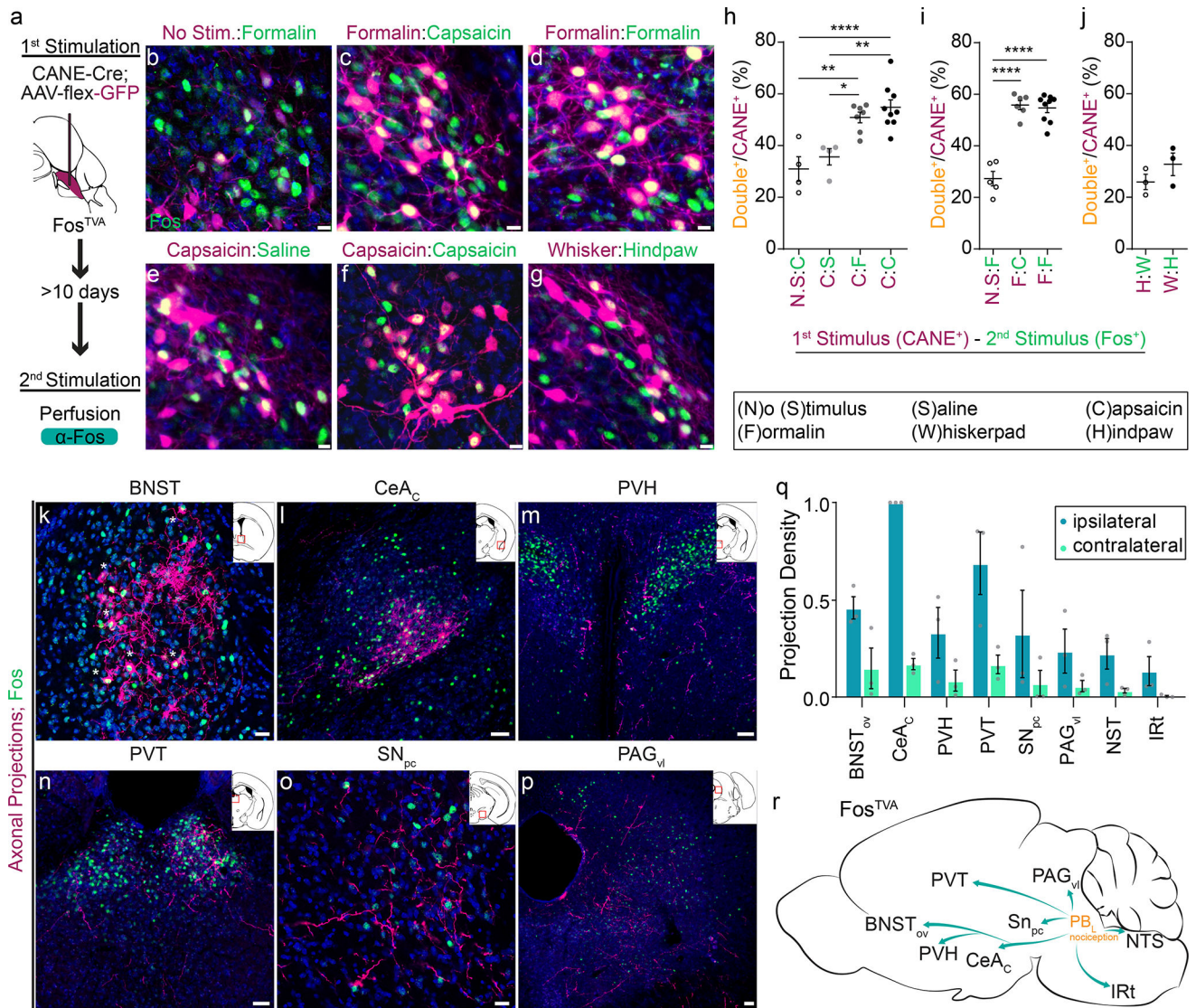


**Figure 2. Capturing and mapping the axonal projection targets of PB<sub>L</sub>-nociceptive neurons**  
(a) Schematic illustration of strategy to express GFP in nociceptive relay PB<sub>L</sub> neurons in Fos<sup>TVA</sup> mice using CANE.

(b-g) Examination of CANE-captured neurons activated by the first stimulus (magenta) versus Fos<sup>+</sup> neurons activated by the second stimulus (green) in the PB<sub>L</sub>. In all six paradigms, CANE method was used to capture neurons activated by stimulus/no stimulus, and 2 weeks later, Fos was induced by the second stimulus. Blue, DAPI. Scale bars, 10 μm.

(h-j) The percentage of Fos<sup>+</sup> neurons among CANE<sup>+</sup> neurons. Data are mean ± SEM. (from left to right: (h) n=4, 9, 7, 4; one-way ANOVA; \*\*\**P* = <0.0001, \*\**P* = 0.0005, *P* = 0.3952, *P* = 0.3223; \*\**P* = 0.0005, \**P* = 0.0047; *F*<sub>3, 20</sub> = 12.49

(i) n = 5, 5, 9; one-way ANOVA; \*\*\**P* = <0.0001, \*\*\**P* = <0.0001, *P* = 0.6876; *F*<sub>2, 17</sub> = 52.17

(j) n = 3, 3; two-tailed unpaired student's *t* test; *P* = 0.2759; *t*<sub>3,505</sub> = 1.289).

(k-p) Representative images of axonal projections from captured formalin activated PB<sub>L</sub> (magenta) in several brain nuclei expressing Fos (green) induced by formalin. (Inset:



Schematic of coronal view of location [in red box] in brain). \* in panel k denotes very large terminal boutons from labeled PB<sub>L</sub> axons in BNST, some of boutons surround the Fos<sup>+</sup> BNST neuron cell bodies.

(q) Quantification of normalized density of innervations (total pixels divided by the area of each nucleus; n = 3). All data shown are mean ± SEM.

(r) Schematic summary for output targets of PB<sub>L</sub>-nociceptive neurons. BNST, bed nucleus of the stria terminalis; PVH, paraventricular hypothalamic nucleus; PVT, paraventricular nucleus of the thalamus; CeA<sub>C</sub>, central amygdalar nucleus, capsular part; SN<sub>PC</sub>, substantia nigra pars compacta; PAG<sub>vl</sub>, ventrolateral periaqueductal gray; NST, nucleus solitary tract; IRt, intermediate reticular tract. Scale bars, (k, o) 20 μm. (l-n, p) 50 μm. (n = 3) Data are mean ± SEM.

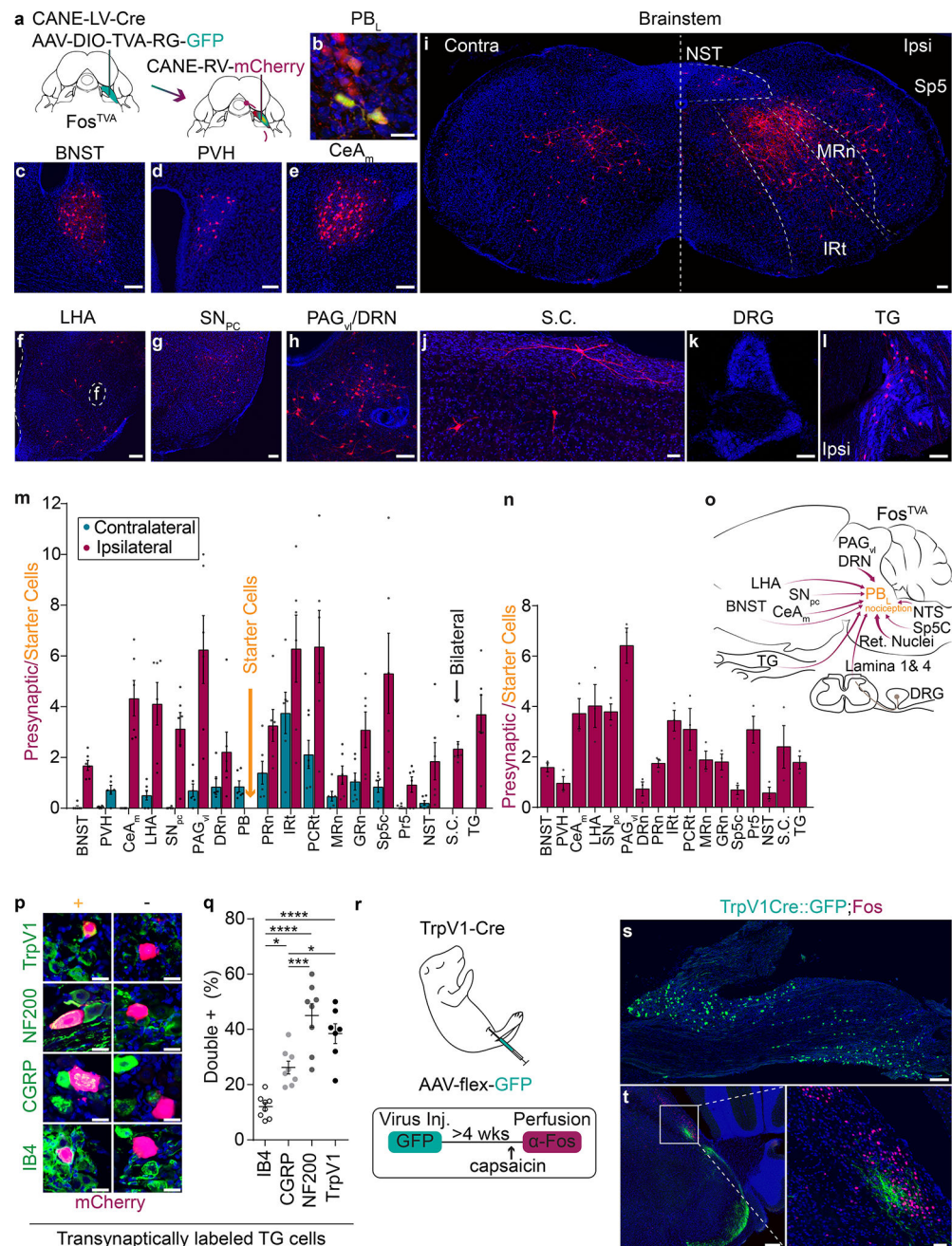


**Figure 3. Transsynaptic labeling of presynaptic neurons for PB<sub>L</sub>-nociceptive neurons reveals the direct TG→PB<sub>L</sub> pathway**

(a) Schematic illustration for transsynaptic tracing of presynaptic inputs to PB<sub>L</sub>-nociceptive neurons.

(b) Representative image of CANE-RV-mCherry-infected PB<sub>L</sub>-nociceptive neurons. Green, PB<sub>L</sub>-nociceptive neurons expressing TVA and RG. Red, RV-mCherry<sup>+</sup>. Yellow, starter cells. Scale bar, 10 μm.

(c-l) Representative images of transsynaptically labeled neurons in several brain regions. Scale bars, (c-h, k-l) 50 μm (i) 100 μm (j) 20 μm

(m) Quantification of transsynaptically labeled neurons in each brain area contralateral (teal) and ipsilateral (magenta) to injected site after whisker pad formalin injection and (n) after hindpaw formalin injection. The value is normalized against the number of starter neurons and averaged across animals. Data are mean  $\pm$  SEM (n = 6; n = 3).

(o) Schematic summary for input sources for PB<sub>L</sub>-nociceptive neurons. BNST, bed nucleus of the stria terminalis; PVH, paraventricular of the hypothalamus; LHA, lateral hypothalamus; CeA, central amygdalar nucleus, medial; SN<sub>PC</sub>, substantia nigra pars compacta; PAG, periaqueductal gray; DRN, dorsal raphe nucleus; Reticular Nuclei: (PRn, pontine reticular nuclei; IRt, intermediate reticular tract; PCRt, parvicellular reticular tract, MRn, medullary reticular nuclei; GRn, gigantocellular reticular nuclei); NST, nucleus solitary tract; Sp5C, trigeminal nucleus, caudalis; TG, trigeminal ganglion; DRG, dorsal root ganglion. S.C., spinal cord (dorsal horn).

(p) Molecular characterization of transsynaptically labeled trigeminal ganglion (TG) neurons. Green; bottom to top: IB4<sup>+</sup>, CGRP<sup>+</sup>, NF200<sup>+</sup>, TrpV1<sup>+</sup>. Left, colocalized transsynaptically labeled TG neurons. Right, non-colocalized labeled TG neurons. Scale bar, 20  $\mu$ m.

(q) Percentage of transsynaptically labeled trigeminal ganglion neurons expressing IB4, CGRP, NF200, or TrpV1. (n = 8; one-way ANOVA; \**P* = 0.0135, \*\* \**P* = 0.0008, \**P* = 0.0468, \*\*\* \**P* = <0.0001, \*\*\* \**P* = <0.0001, *P* = 0.4653; *F*<sub>3, 27</sub> = 22.7). Data are mean  $\pm$  SEM.

(r) Schematic illustration and timeline of intraperitoneal injection in 1–2 day old TrpV1-Cre pup with AAV9-CAG-flex-GFP. Four weeks after injection, TrpV1Cre::GFP mouse was injected with capsaicin in the whisker pad and stained for Fos (n = 4 mice).

(s) Representative image of trigeminal ganglion with TrpV1Cre::GFP<sup>+</sup> neurons. Scale bar, 200  $\mu$ m.

(t) Representative image of PB<sub>L</sub> with TrpV1Cre::GFP<sup>+</sup> axon terminals (Green) and capsaicin-induced Fos<sup>+</sup> neurons (magenta). Scale bar, 50  $\mu$ m (high mag).



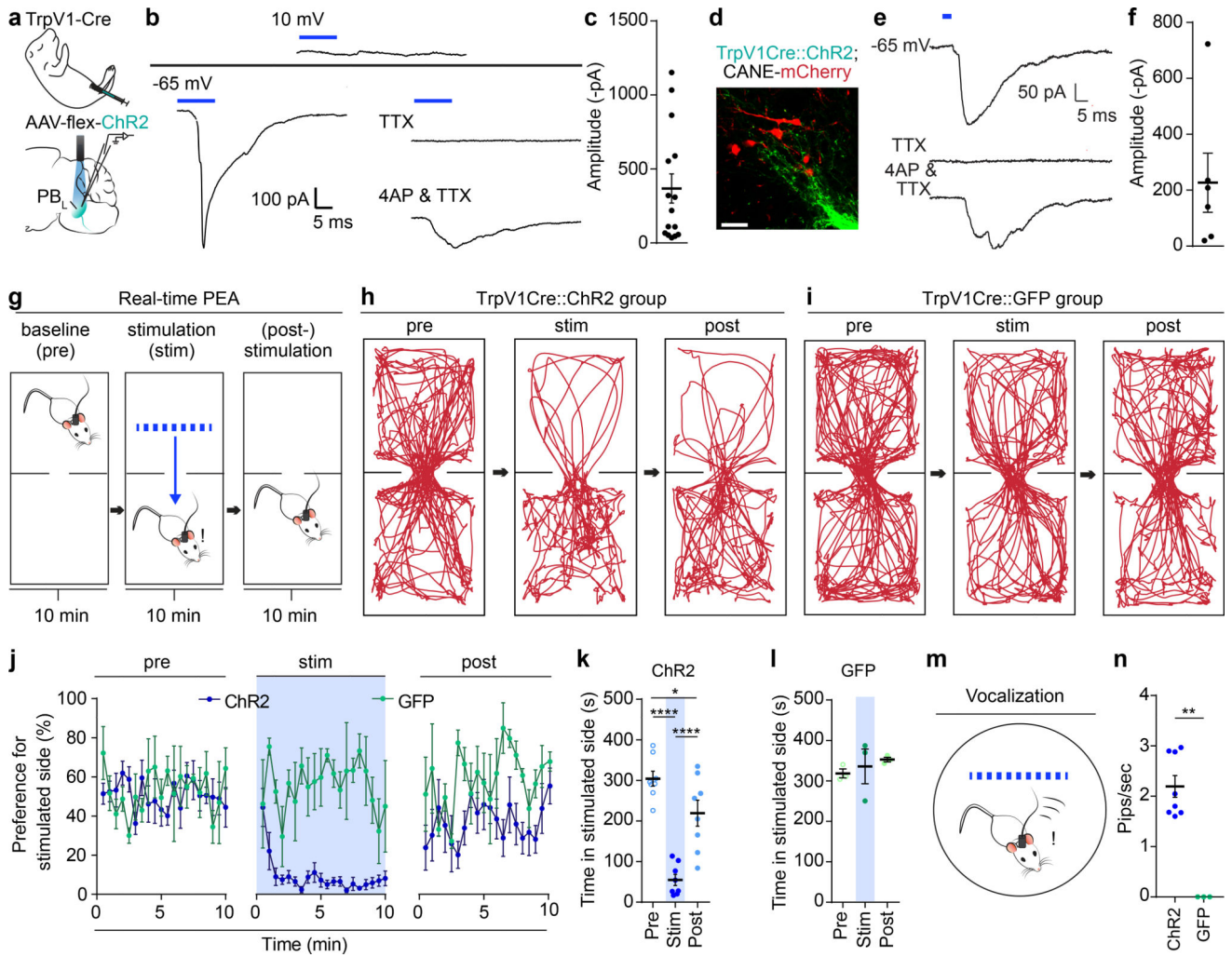


**Figure 4. Optogenetic activation of TrpV1-Cre<sup>+</sup> sensory axons activates PB<sub>L</sub>-nociceptive neurons and elicits aversive behavior and stress calls in a real-time place escape/avoidance task**

(a) Schematic illustration of intraperitoneal injection of a 1–2 day old TrpV1-Cre pup ( $n = 3$ ), followed by optogenetic-assisted whole cell patch-clamp recording from a PB<sub>L</sub> neuron in acute brain slices

(b) Representative traces from a cell showing no light-evoked IPSC at a holding potential of 10mV, but observed to have light-evoked EPSC at a holding of  $-65$ mV. Cell, held at  $-65$ mV, was bath applied with  $1\mu\text{M}$  TTX, followed by  $100\mu\text{M}$  4-AP and  $1\mu\text{M}$  TTX, showing a light-evoked monosynaptic EPSC.

(c) Averaged current amplitude is shown. Data are mean  $\pm$  SEM. (closed circles, individual cells,  $n = 15$ ).

(d) Representative high-mag image of TrpV1Cre::ChR2<sup>+</sup> axon terminals and CANE-RV-mCherry captured PB<sub>L</sub>-pain neurons. ( $n = 3$  mice; Scale bar,  $50\mu\text{m}$ ).

(e) Representative of an mCherry<sup>+</sup> PB<sub>L</sub>-pain neuron recorded to have light-evoked EPSC at a holding of  $-65$ mV. Cell was bath applied with  $1\mu\text{M}$  TTX, followed by  $100\mu\text{M}$  4-AP and  $1\mu\text{M}$  TTX, showing a light-evoked monosynaptic EPSC.

- (f) Averaged current amplitude is shown. Data are mean  $\pm$  SEM. (closed circles, individual cells,  $n = 6$ ).
- (g) Schematic illustration of real-time place escape/avoidance (PEA) test.
- (h) Representative spatial tracking map showing the location of an experimental mouse before, during, and after optogenetic stimulation of TrpV1Cre::ChR2<sup>+</sup> axon terminals in the PB<sub>L</sub> in the preferred chamber.
- (i) Representative spatial tracking map showing the location of a control mouse before, during, and after illuminating TrpV1Cre::GFP<sup>+</sup> axon terminals in the PB<sub>L</sub> in the preferred chamber.
- (j) Percentage of preference (per 30 seconds) the experimental and control groups had before, during, and after optogenetic stimulation ( $n = 8$  &  $3$ ) shown across time (min). Data are mean  $\pm$  SEM.
- (k) Quantification of time the TrpV1Cre::ChR2 group spent in preferred chamber before, during, and after optogenetic stimulation ( $n = 8$  one-way repeated measures ANOVA; \*\*\*  $P = <0.0001$ , \*  $P = 0.0128$ , \*\*\*  $P = <0.0001$ ;  $F_{2, 14} = 49.41$ ). Data are mean  $\pm$  SEM.
- (l) Quantification of time the TrpV1Cre::GFP group spent in preferred chamber before, during, and after light illumination ( $n = 3$ ; one-way repeated measures ANOVA;  $P = 0.8867$ ,  $P = 0.6377$ ,  $P = 0.8886$ ;  $F_{2, 6} = 0.4412$ ). Data are mean  $\pm$  SEM.
- (m) Schematic illustration of vocalization recording chamber.
- (n) Quantification of frequency of pips induced by optogenetic stimulation of TrpV1Cre::ChR2 (experimental) or TrpV1Cre::GFP (control) axon terminals in the PB<sub>L</sub>. Data are mean  $\pm$  SEM. (ChR2,  $n = 8$ ; GFP,  $n = 3$ ; two-tailed unpaired student's  $t$  test; \*\*  $P = <0.0001$ ;  $t_7 = 10.13$ ).

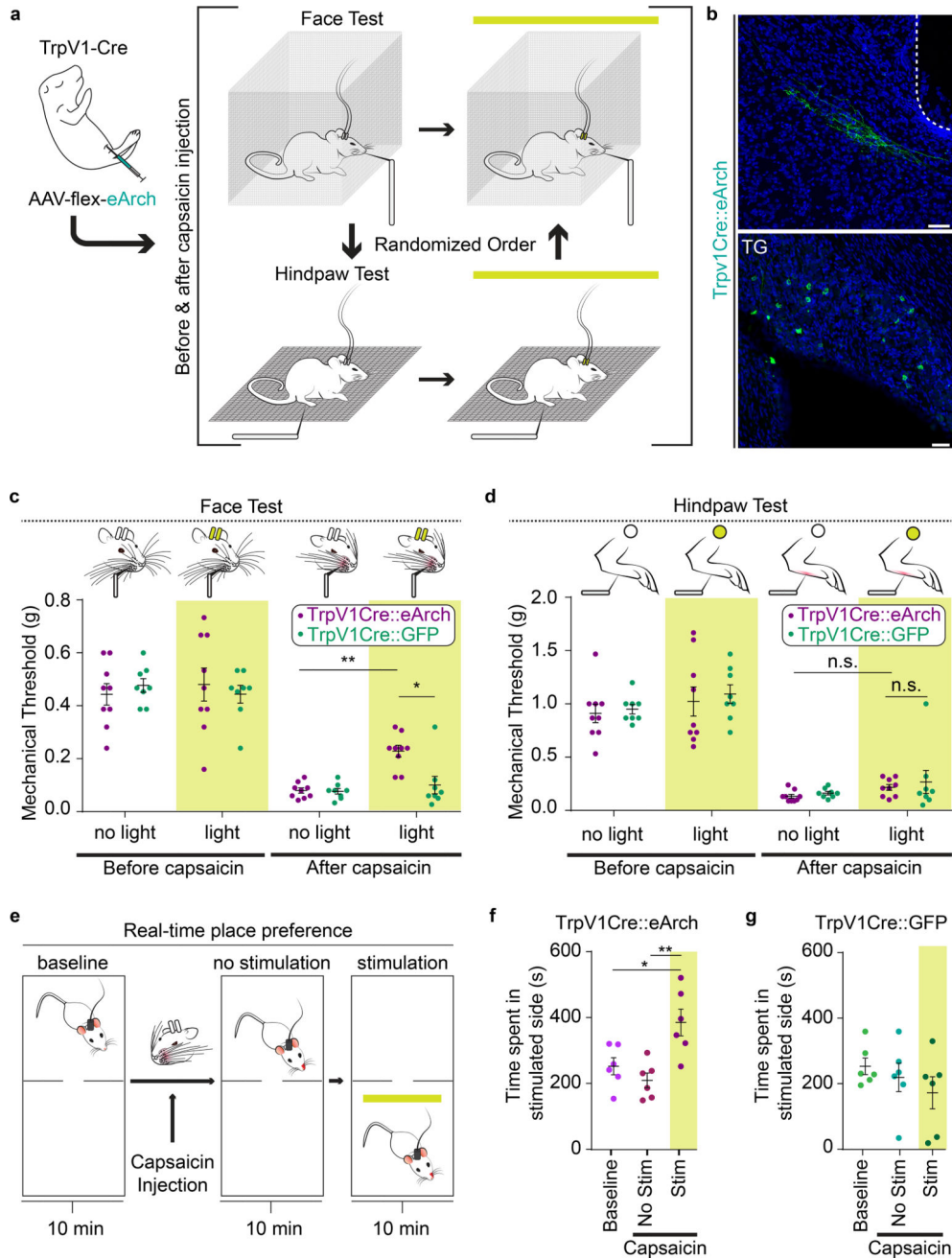


**Figure 5. Optogenetic silencing of TrpV1-Cre<sup>+</sup> axon terminals in PB<sub>L</sub> selectively reduces face allodynia after capsaicin injection**

(a) Schematic illustration of intraperitoneal injection of a 1–2 day old TrpV1-Cre pup followed by a face and hindpaw von Frey tests in the same individual mice in TrpV1Cre::eArch (n = 9) and TrpV1Cre::GFP groups (n = 8). The order of face versus hindpaw tests was randomized. Each mouse was tested before and after 10  $\mu$ L 4% capsaicin was injected into either face or hindpaw.

(b) Representative post-hoc image of TrpV1Cre::eArch<sup>+</sup> axon terminals in PB<sub>L</sub> and labeled TrpV1Cre::eArch<sup>+</sup> cell bodies in TG (n = 9 mice; Scale bars, 50  $\mu$ m).

- (c) Quantification of mechanical thresholds of face withdrawal responses in von Frey tests. Measurements were taken before and after capsaicin injection into right whisker pad, as well as without and with optogenetic silencing in TrpV1Cre::eArch (n = 9) or in control TrpV1Cre::GFP groups (n = 8, two-way repeated measures ANOVA; (eArch vs. GFP)  $P = >0.9999$ ,  $P = >0.9999$ ,  $P = >0.9999$ ,  $*P = 0.0440$ ; (no light vs light) eArch:  $P = >0.9999$ ,  $**P = 0.0046$ , GFP:  $P = >0.9999$ ,  $P = >0.9999$ ;  $F(3, 45) = 2.671$ ). Data are mean  $\pm$  SEM.
- (d) Quantification of mechanical thresholds of hindpaw withdrawal responses in von Frey tests. Measurements were taken before and after capsaicin injection into right hindpaw, as well as without and with optogenetic silencing in TrpV1Cre::eArch (n = 9) or in TrpV1Cre::GFP groups (n = 8, two-way repeated measures ANOVA; (Arch vs. GFP)  $P = >0.9999$ ,  $P = >0.9999$ ,  $P = >0.9999$ ,  $>0.9999$ ; (no light vs light) Arch:  $P = >0.9999$ ,  $P = >0.9999$ , GFP:  $P = >0.9999$ ,  $P = >0.9999$ ;  $F(3, 45) = 0.03048$ ). Data are mean  $\pm$  SEM.
- (e) Schematic illustration of real-time place preference (RTPP) test of mouse injected with capsaicin into left whisker pad.
- (f) Quantification of time the experimental group spent in non-preferred chamber before capsaicin, after capsaicin, and without or with optogenetic silencing (n = 6 one-way repeated measures ANOVA;  $P = 0.5356$ ,  $*P = 0.0174$ ,  $**P = 0.0031$ ;  $F_{2, 10} = 10.92$ ). Data are mean  $\pm$  SEM.
- (g) Quantification of time the control group spent in non-preferred chamber before capsaicin, after capsaicin, and without or with optogenetic silencing (n = 7; one-way repeated measures ANOVA;  $P = 0.7320$ ,  $P = 0.2086$ ,  $P = 0.5537$ ;  $F_{2, 10} = 1.695$ ). Data are mean  $\pm$  SEM.